(12) INTERNATIONAL APPLICATION PUBLISHED UNDER THE PATENT COOPERATION TREATY (PCT)

(19) World Intellectual Property Organization
International Bureau

(43) International Publication Date
7 June 2001 (07.06.2001)

PCT

(10) International Publication Number
WO 01/40776 A1

(51) International Patent Classification[7]: G01N 21/35, A61B 5/00

(21) International Application Number: PCT/US00/32830

(22) International Filing Date: 4 December 2000 (04.12.2000)

(25) Filing Language: English

(26) Publication Language: English

(30) Priority Data:
60/168,529 2 December 1999 (02.12.1999) US

(71) Applicant *(for all designated States except US)*: **JOHNS HOPKINS UNIVERSITY** [US/US]; School of Medicine, 111 Market Place, Suite 906, Baltimore, MD 21202 (US).

(72) Inventor; and

(75) Inventor/Applicant *(for US only)*: **WILSON, David, A.** [US/US]; 9426 Oak White Road, Baltimore, MD 21236 (US).

(74) Agent: **MOLAN, Robert, A.**; Nixon & Vanderhye P.C., Suite 800, 1100 North Glebe Road, Arlington, VI 22201-4714 (US).

(81) Designated States *(national)*: AE, AG, AL, AM, AT, AU, AZ, BA, BB, BG, BR, BY, BZ, CA, CH, CN, CR, CU, CZ, DE, DK, DM, DZ, EE, ES, FI, GB, GD, GE, GH, GM, HR, HU, ID, IL, IN, IS, JP, KE, KG, KP, KR, KZ, LC, LK, LR, LS, LT, LU, LV, MA, MD, MG, MK, MN, MW, MX, MZ, NO, NZ, PL, PT, RO, RU, SD, SE, SG, SI, SK, SL, TJ, TM, TR, TT, TZ, UA, UG, US, UZ, VN, YU, ZA, ZW.

(84) Designated States *(regional)*: ARIPO patent (GH, GM, KE, LS, MW, MZ, SD, SL, SZ, TZ, UG, ZW), Eurasian patent (AM, AZ, BY, KG, KZ, MD, RU, TJ, TM), European patent (AT, BE, CH, CY, DE, DK, ES, FI, FR, GB, GR, IE, IT, LU, MC, NL, PT, SE, TR), OAPI patent (BF, BJ, CF, CG, CI, CM, GA, GN, GW, ML, MR, NE, SN, TD, TG).

Published:
— *With international search report.*

For two-letter codes and other abbreviations, refer to the "Guidance Notes on Codes and Abbreviations" appearing at the beginning of each regular issue of the PCT Gazette.

WO 01/40776 A1

(54) Title: METHOD OF MEASURING TISSUE HEMOGLOBIN SATURATION USING GAUSSIAN DECOMPOSITION

(57) Abstract: The constituents of cerebral tissues that contribute to light absorbency, i.e., oxyhemoglobin, deoxyhemoglobin, water, lipid, cytochrome oxidase and a component for characterising light loss due to scattering, are further characterized and used to construct a model system that emulates cerebral tissue reflectance spectra in a variety of conditions. Using this model system in a reverse mode, compound spectra collected from brain tissue are decomposed into individual spectra features. The values for features attributable to oxyhemoglobin and deoxyhemoglobin are then used to construct a ratio that quantifies the percentage of total hemoglobin that contains oxygen. Because the major portion of light, collected by the detecting element of the equipment has transited through brain tissue, this ratio becomes a quantitative measure of brain tissue hemoglobin saturation. The decomposition analysis method is generally applicable to a variety of tissues besides brain tissue.

METHOD OF MEASURING TISSUE HEMOGLOBIN SATURATION USING GAUSSIAN DECOMPOSITION

Field of the Invention

The present invention relates to determining hemoglobin saturation in tissue, and, in particular, to a method of using gaussian decomposition of diffuse reflectance spectra to determine hemoglobin saturation in tissue.

Background of the Invention

The principal function of hemoglobin is to transport oxygen from the lungs to body tissues. If the transport process is temporarily interrupted at any step between the binding of oxygen to hemoglobin in the lungs and its final conversion to water in the cells of the tissue, the result will be a decrease in intracellular adenosine triphosphate, a molecule used to store energy for cellular processes. If the interruption continues over a prolonged time interval, the cells' inability to perform routine cellular functions will eventually result in cell death.

Numerous pathologic mechanisms can reduce the amount of oxygen in tissues (tissue hypoxia). Moreover, a number of surgical

procedures, designed to repair or alter parts of a body's circulation system, employ techniques that intentionally interrupt oxygen transport.

In the 1970s, Ohmeda introduced the pulse oximeter. This is an inexpensive instrument that can be routinely applied to patients in a variety of settings; at the patients bedside, in the operating room, and has even become standard equipment on emergency vehicles. The device allowed medically trained personnel, for the first time, to monitor a patient's arterial hemoglobin saturation, without having to place an arterial line. The instrument has achieved wide success and has become entrenched as a standard for medical care. However, arterial hemoglobin saturation is a parameter that conveys to the physician how well the heart and lungs are functioning in their ability to keep blood oxygenated. It does not provide any information about how well the tissues that use the oxygen are performing, nor does it provide information about their status. It simply provides the physician with a number that relates to the amount of oxygen that is available to tissues, provided the tissues are functioning normally and have available to them a means of drawing on this oxygen pool.

In instances where blood pressure is low as a result of hemorrhage, blood may be adequately oxygenated, but unavailable to tissues because of a low perfusion pressure, or because the body has restricted the oxygen

supply to that tissue in an attempt to conserve other organs, such as the heart and brain. Another instance where arterial hemoglobin saturation is of no value is in the case of endartarectomy. In this common medical procedure designed to physically remove placque from the inner surfaces of blood vessels supplying the brain, a surgeon may choose to apply a clip across the affected side as he performs the procedure. He does this to prevent blood loss and experience has shown that the clip can remain in place for a finite period of time before it has to be removed to prevent damage to the brain. The amount of oxygen that the brain on the operated side receives during the procedure is dependent upon the degree to which blood vessels cross-connected to the unoperated side can supply the affected side. The amount of "collateralization" is dependent upon numerous factors. Among these are the age of the patient, the size and number of vessels, and the degree and stage of disease. Presently, the surgeon relies upon indirect measures of stress to determine when and if the brain's oxygen supply is compromised. These indirect measures are other technologies that monitor aspects of function, such as evoked potentials, or electroencephalographic activity. But, these measures "report" deficiency only *after* function is compromised. Presently, there are no available technologies in common clinical use that are capable of forewarning the physician or surgeon that a state of oxygen deficiency is either developing, or exists, in a specific organ's tissues.

A number of laboratories are presently working to develop "tissue oximeters". Early efforts focused upon oximeters directed at monitoring the degree of saturation of hemoglobin in brain tissue using optical methods that that can be performed noninvasively. Focus has been on brain tissue, not only because of the importance of this organ, but also because of the apparent advantages offered by the anatomy of the head. The brain is relatively near the surface of the skin and is separated from the environment by only a thin layer of optically transparent bone that contains a minimal amount of blood. Measuring brain tissue hemoglobin saturation has turned out to be a not so easy task to perform.

At least six different methodologies have been developed and used to extract hemoglobin related information from brain tissue spectra. The goal of each of these approaches is to quantify the two components of hemoglobin individually, and in such a manner, as to allow the components to be recombined in the form of a ratio that describes the percentage of hemoglobin, contained within an optical field, that is combined with oxygen. Generally, the methods that have emerged to perform this task have done so from new insights or from new theoretical prospectives that offer a potential solution to the tissue hemoglobin saturation problem. Accordingly, instrumentation has been tailored to the specific requirements of the analytical solution conceived.

Simple, multi-wavelength, absorbency-based algorithms

The distinguishing characteristic of approaches under this category is that only optical attenuation is used in the computations required to obtain a numeric solution. Typically, this information is input into an algorithm in the form of optical density measurements monitored at two to four select wavelengths. Historically, *in vivo* multi-wavelength spectroscopy was first employed as a means of characterizing the *in vivo* redox state of cytochrome oxidase. To do this, it was recognized that the various forms of hemoglobin had to be characterized as well, because each overlies the cytochrome oxidase spectrum. While it remains a goal of most *in vivo* spectroscopists to develop a method that fully characterizes cytochrome oxidase, most of the recent efforts have focused upon ways to fully characterize hemoglobin concentration change. Multi-wavelength absorbency based spectroscopy is attractive because it requires simple and straight-forward mathematical computations. Instrumentation design is relatively uncomplicated and economically feasible. A weakness of multi-wavelength absorbency-based methods is that they employ no means of characterizing light lost from the sampled tissue by light scattering processes, and thus, in principle, can only report changes in constituent concentration from an arbitrarily established baseline.

A number of instruments marketed today employ simple, multi-wavelength, absorbency technology. These include products by the Somanetics Corporation (INVOS 3100 and 4100), the Hamamatsu Corporation (NIRO 500 and 1000), and NIM, Incorporated (Runman). Two other instruments recently appeared in reports from the literature, but there is little public information regarding the nature of their technologies or methods for analytical solution. These are instruments being developed by Hutchinson Technologies, Inc. of Hutchinson, MN and by the Tostec Co., Inc. of Tokyo, Japan. All of these instruments claim to be able to provide trend information that is based upon an initial baseline setting and all claim to provide an accurate measure of tissue hemoglobin saturation. Because the Somanetics INVOS 3100 instrument was the first commercially available instrument in this country, it has undergone the most evaluation. These studies have been disappointing in some respects, for the clinician's confidence in this potentially useful technology has waned in the aftermath. The INVOS 3100 instrument has been revised and new reports on the INVOS 4100 are beginning to appear.

Derivative spectroscopy

If it can be assumed that light scattering primarily influences baseline absorbency, *i.e.*, that light scattering is not strongly wavelength

dependent, then baseline influences can be nulled by derivatizing spectra. In 1989, it was shown that it is possible to compute a parameter, using derivatized spectra, that correlates highly with brain tissue hemoglobin saturation. While the method was demonstrated to be feasible, it was at that time believed to be impractical for commercialization because the algorithm was not portable to other instruments, *i.e.,* the coefficients employed were instrument specific.

Pseudo-random modulated code spectroscopy (PRM)

PRM technology was originally developed for use in satellite technologies to measure the height of the ocean surface from space. PRM spectroscopy evolved as a means of quantifying the much shorter distances that photons travel in brain tissue. The PRM technique relies upon a randomized sequence of light pulses of varying, but known, widths. These pulse sequences are unique and when repetitively transmitted into tissue and their emergence from the tissue is measured, the sequences can be identified using autocorrelation analysis. By comparing the input and output sequences, a time-shifted difference, or time-of-travel for photons through tissue, can be characterized. The scattering and absorption coefficients (μ_s and μ_a, respectively) can be extracted from X^2 curve fitting the convolution of the instrument impulse

response function with the theoretical reflectance function of μ_s and μ_a, respectively to the measured photon migration profile. Blood oxygenation can be measured by performing the calculations at two wavelengths and ratioing the absorption coefficients found there. The advantages of the PRM technique is that it can be performed using instrumentation that is relatively inexpensive to manufacture and safe to use.

Time-resolved spectroscopy (TRS)

Because tissue is an effective multiple scatterer of light, the light pathlength needed to perform quantitative calculations of hemoglobin concentration is normally unknown. In 1988, it was shown that it was possible to calculate a mean pathlength by measuring the time it takes energy, pulsed in picosecond increments, to traverse the head. Time-resolved spectroscopy has become a standard in the field of *in vivo* spectroscopy because of its ability to measure pathlength directly. However, it has not been demonstrated to be a method suitable for clinical use for several reasons. TRS requires using very short laser pulses and ultrafast photon counting equipment. Consequently, the delivery of light and the recovery of light from tissues requires equipment that is expensive, bulky, and requires a high degree of maintenance.

Moreover, the intrinsic high peak power of picosecond lasers requires further operational precautions.

Phase-modulation, or frequency-resolved spectroscopy (FRS)

FRS followed as a natural application of previous experiences with radar and altimeter development. A coded light signal (typically sinusiodal or square in shape) is injected into tissue. Photon diffusion encodes the tissue characteristics in the timing of the delayed, received pulse and in the intensity of the time profile. Thus, instead of receiving a clean replicate of the transmitted pulse, the returned signals are spread out over time and are diminished in amplitude. The signal information is decoded using procedures similar to that described previously for the PRM method. This technique, like that of PRM, requires relatively inexpensive equipment to generate encoded light signals. It is safe to use in that only small amounts of energy are required (microwatts). It provides a measure of pathlength, thus allowing constituent concentration to be computed directly from the Beer-Lambert relationship. The disadvantage of the method is that it may be more susceptible to noise than is PRM. Also, like PRM methods, FRS relies upon a mathematical model of photon migration in a semi-infinite medium to recover tissue absorption coefficients.

Two instrument designs have been based on the FRS methodology. The NIM instrument (PMD 4002, NIM Incorporated, Philadelphia, PA) incorporates three tissue-illuminating wavelengths, and a fourth, reference wavelength. It is a hybridized design, thus, incorporating both FRS and multi-wavelength, absorbance-based methodologies. It has been tested, both *in vitro*, and *in vivo,* in animal experiments. Tissue hemoglobin saturation measurement made with this instrument system show an excellent linear correlation with tissue hemoglobin saturation estimated from measurements made on whole blood. Another instrument is presently marketed by ISS, Inc. This instrument has not undergone rigorous evaluation. It is a two-wavelength, four-channel device.

Photoacoustic spectroscopy

When light energy is absorbed by molecules of a tissue, heat is liberated in the process. This quickly results in thermal expansion of the surrounding tissue, which, in turn, is followed by a rapid collapse to the original state. The result is an acoustic signal that can be "heard" in the ultrasound range. The amplitude of the acoustic signal is proportional to the amount of light absorbed. Most importantly, the amplitude of the signal is related to the total amount of light absorbed, including that which is contained in the photon migration path. It has been demonstrated that this method is feasible when applied to biologic tissue.

However, while the method is advantageous in being insensitive to changes in the light scattering properties of tissue, it was later found that the useable signal originates close to the surface of the tissue, and was, thus, not suited for measuring changes in tissue constituent composition in deep structures.

At least six different approaches have been used to extract constituent information from spectra collected from tissues. All of the techniques described use procedures that are noninvasive and non-damaging to the tissue. With the exception of TRS, most of these methods can be performed using equipment that is relatively inexpensive to construct and maintain. TRS, FRS, and PRM technologies are at the forefront of development because they incorporate solutions for measuring pathlength, a necessary component of the Beer-Lambert solution for absolute constituent concentration. Multi-wavelength methodologies have become established for trending measurements, but they cannot be used for quantitative measurement. All methods are susceptible to noise because of the low light level requirements established for patient safety. Excepting derivative spectroscopy, all methods are multi-wavelength and use absorbency changes occurring at only two to four points within the entire near infrared ("NIR") range. Hence, all methods, to a greater or lesser extent, are subject to how well

absorbency changes at these wavelengths reflect changes occurring within the monitored tissue.

Summary of the Invention

An object of the present invention is to provide a method of measuring tissue oxygenation that can be performed using instrumentation that is portable and inexpensive to make, such that bedside and field measurements of this parameter can be quickly and accurately made.

The present invention is a method for decomposing compound diffuse reflectance spectra, collected from tissue, such as brain tissue, into discrete constituents that can then be used to compute tissue hemoglobin saturation. The present invention requires a spectrometer capable of collecting full absorption spectra in the NIR band and a computer for data acquisition and processing. Because constituents other than hemoglobin must be quantified in the process of extracting this information, the method additionally yields qualitative information about these constituents. In the case of brain tissue, these secondary parameters are related to the water content of the brain tissue, the redox state of brain tissue cytochrome oxidase, cerebral tissue lipid content, and the brain's light scattering properties. The secondary constituent characterizations

are qualitative, but the values can be used for trending purposes, or for comparing relative amounts between tissue regions or between brain hemispheres, when collected and analyzed as a function of optical path length. The method of the present invention can be further developed to quantify all of these secondary parameters.

The constituents of cerebral tissues that contribute to light absorbency, *i.e.,* oxyhemoglobin, deoxyhemoglobin, water, lipid, cytochrome oxidase and a component for characterizing light loss due to scattering, are further characterized and used to construct a model system that emulates cerebral tissue reflectance spectra in a variety of conditions. Using this model system in a reverse mode, compound spectra collected from brain tissue are decomposed into individual spectral features. The values for features attributable to oxyhemoglobin and deoxyhemoglobin are then used to construct a ratio that quantifies the percentage of total hemoglobin that contains oxygen. Because the major portion of light collected by the detecting element of the equipment has transited through brain tissue, this ratio becomes a quantitative measure of brain tissue hemoglobin saturation. Because it is a ratio, it does not require a knowledge of *in vivo* molar absorption coefficients and it is relatively pathlength insensitive .

BRIEF DESCRIPTION OF THE DRAWINGS

FIGURE 1 is a graph showing the absorption spectra of oxygenated and deoxygenated hemoglobin.

FIGURE 2 is a block diagram of the instrumentation used to carry out the method of the present invention.

FIGURE 3 is a graph showing NIR prediction versus measured tissue hemoglobin saturation.

FIGURE 4 is a graph showing that the oxyhemoglobin feature increases during hypoxic-hypoxia.

FIGURE 5 is a graph showing that adding linkage between the 760 nm and 930 nm features corrects the directional error in recovered oxyhemoglobin

FIGURE 6 is a graph showing the ratio of oxyhemoglobin absorption to absorption attributable to total hemoglobin is proportional to tissue hemoglobin saturation.

FIGURE 7 is a graph showing that the ratio of oxyhemoglobin absorption to absorption attributable to total hemoglobin can be adjusted

using two coefficients to provide a numerical predictor of brain tissue hemoglobin saturation.

FIGURE 8 is a graph showing the best and worst case fits to absorption spectra and the error of prediction.

FIGURE 9 is a graph showing that feature absorbency is optrode separation distance dependent.

FIGURE 10 is a graph showing tissue hemoglobin saturation, measured by gaussian decomposition methods is optode separation distance independent.

FIGURE 11 is a graph showing water corrected spectra from bacon and white matter.

FIGURE 12 is a graph showing the result of fitting the $HbSat_{bt}$ ratio to computed tissue hemoglobin saturation.

FIGURES 13A and B are graphs showing the effect linking two deoxyhemoglobin features has on the total hemoglobin attenuation.

FIGURE 14 is a graph showing an absorption spectrum from cat head and the goodness-of-fit provided by Model C.

FIGURE 15 is a graph showing an absorption spectrum from gastrocnemius and the goodness-of-fit provided by Model C.

DESCRIPTION OF THE PREFERRED EMBODIMENT

An absorption spectrum is a plot of how light within a range of energies is absorbed by molecules. For pure substances (constituents) in a dilute solution, the amount of light absorbed at any particular energy level is proportional to the concentration of the constituent in the solution. The spectrum for a particular constituent can be thought of as being analogous to a fingerprint, with it's shape being it's most distinguishing characteristic. It may be simple or complex, depending on the number of absorbers present, but it is uniquely shaped. For mixtures of constituents in a solution, a compound spectrum is observed. This compound spectrum results from the summation of all absorbencies by all of the substances contained within the mixture. Compound spectra can be broken down into basic elements if the features of all of the possible constituents are known.

The Beer-Lambert law states that absorption, A, at a selected wavelength, λ, is proportional to the concentration of a constituent, c, and

the pathlength, L, through which the light travels during measurement, so that:

$$A(\lambda) = \varepsilon(\lambda)cL \quad (1)$$

where $\varepsilon(\lambda)$ is the molar absorption coefficient and is wavelength dependent. For many absorbers, $\varepsilon(\lambda)$ has the characteristics of a gaussian probability distribution and is the property that lends shape to the absorption spectrum. For simple constituents (constituents with a single absorbing center) having these properties, an equation of the form

$$[A]_{\lambda min..\lambda max} = \varepsilon_{max}\, c\, L\, EXP((-0.5((\lambda-\lambda_c)/FWHM)^2) \quad (2)$$

may be written, where $[A]_{\lambda min..\lambda max}$ is an array, or range of absorbencies, or an absorption spectrum, ε_{max} is the maximum value of the absorption spectrum within the range, *FWHM* is the width of the spectrum at $1/2*\varepsilon_{max}$, and λ_c is the wavelength around which the spectral range is centered. Complex spectra, *i.e.* constituents with multiple absorbing centers, can be described as a summed representation of equation 2, wherein each center is described. Equation 2, or its summed representation, thus describes constituent shape; a property that is unique for every substance. Note that when λ_c equals λ, the terms inside the brackets reduce to zero and the exponentiated portion of the equation

takes on the value of unity. In this special case, equation 2 reduces to equation 1. It follows that c may be determined from $[A]_{\lambda min..\lambda max}$, if ε_{max}, L, $FWHM$, and λ_c are known.

Decomposition of compound spectra requires an *a priori* knowledge of the absorption properties of all constituents that absorb within the specified region of optical monitoring. This information may be termed a spectral feature database. Because some compounds have similar features at similar energy locations, rules regarding how features interact must also be known before they can be separated properly. For example, the deoxyhemoglobin molecule has two absorbencies in the 700-1100 nm NIR band, one of which overlaps with oxyhemoglobin. To separate a compound spectrum containing oxyhemoglobin and deoxyhemoglobin into elemental spectra, a rule is needed indicating that the deoxyhemoglobin contribution to the region overlapping oxyhemoglobin will be a constant fraction of the non-overlapping feature. One other factor must be known. Because photons shone into tissues are also subject to light scattering, the knowledge base must also include rules to account for "apparent" absorption, or light loss. The spectra feature database, used in conjunction with a rule set and a definition regarding how light scattering contributes to baseline absorption, is herein defined as a knowledge base or, in engineering terminology, a model

system. It follows that, if the model system completely describes the real system, then it can be applied to real spectra in a reverse manner and used to derive the relative concentrations of the constituents that contribute to a compound spectrum. A least squares curve fitting procedure is used to adjust the parameters of a model system until the error between the experimental spectrum and the model spectrum is minimized. The individual contributing constituent information can then be recovered.

The constituents of cerebral tissues that contribute to light absorbency are known. According to the present invention, these constituents are further characterized and are used to construct a constrained parameter, model system that emulates cerebral tissue reflectance spectra in a variety of conditions. The knowledge base incorporates information about oxyhemoglobin, deoxyhemoglobin, water, lipid, cytochrome oxidase and includes a component to characterize light loss due to scattering. Using this model system in a reverse mode, compound spectra collected from brain tissue are decomposed into individual spectral features. The values for features attributable to oxyhemoglobin and deoxyhemoglobin are "recovered" and used to construct a ratio that quantifies the percentage of total hemoglobin that contains oxygen. Because the major portion of light has transited through brain tissue, this ratio becomes a quantitative measure of brain tissue

hemoglobin saturation. This has been experimentally verified. The model system was built from spectral information collected in dogs and cats, but is generally applicable to other mammalian species, including man.

One hemoglobin molecule consists of two alpha and two beta heme containing polypeptide chains (globins). Together, the chains form a single molecule with four heme units that is capable of carrying four oxygen molecules. The features present in a sample spectrum of hemoglobin depend on the relative proportion of the number of hemoglobin molecules that contain bound oxygen. In the fully oxygenated form, features of high absorbency are located at 415, 542, 577, and 930 nm. In the deoxygenated form, the features shift location and are located at 431, 555, 760, and 910 nm. Prior work in monitoring brain tissue hemoglobin saturation has focused on identifying the constituents in brain that have absorbing properties in a narrow energy band known as the near-infrared window ("NIR"), *i.e.,* 700 nm to 1100 nm. This is because this energy window contains only weak absorbencies which allows light to penetrate more deeply into tissue than in other parts of the light energy band. The features present in the NIR band, for oxygenated and deoxygenated hemoglobin, are illustrated in Figure 1. Above the upper energy cutoff of the NIR window, *i.e.*, $\lambda < 700$ nm, a

strong absorbency by the visible hemoglobin features prevents light from penetrating deeply. Below the lower energy limit, *i.e.*, $\lambda > 1100$ nm, light is absorbed superficially by a strong water absorbency. At least identifiable features are contained within the NIR window of biological tissues. Three features are attributed to hemoglobin, two to lipid, two to cytochrome oxidase, and three to water. Of the four primary NIR absorbers, water, hemoglobin, cytochrome oxidase, and lipid, water is the most abundant absorber (82% by weight), followed by lipid (~12%), hemoglobin (~0.4%), and cytochrome oxidase (<0.1%).

FIGURE 1 shows the absorption spectra 11 and 12 of oxygenated and deoxygenated hemoglobin, respectively. The spectra 11 and 12 were collected using a fourier transform spectrometer (Model 2000, Perkin-Elmer Corporation). The spectra 11 and 12 were collected in transmittance mode while illuminating a sample of whole blood perfusing through a 0.1 cm pathlength quartz flow-through perfusion cell that had been inserted into an arterial-venous shunt, created in a cat animal model. Hemoglobin saturation during the period when the oxygenated spectrum was collected, measured 98.7% on a benchtop blood gas analyzer (ABL, Radiometer). During collection of the deoxygenated spectrum 12, it measured 25.3%. Both spectra have been post-processed and corrected for instrument tilt and water absorption.

The absorbing properties of hemoglobin have been extensively studied. In normal individuals, the predominant hemoglobin forms are oxyhemoglobin and deoxyhemoglobin, although other forms of the molecule may rise to significant concentrations in unhealthy individuals. In the fully oxygenated state, oxyhemoglobin absorbs light in a broad portion of the NIR band and has a peak absorbency centered at approximately 930 nm. As oxyhemoglobin deoxygenates, absorbency at 930 nm decreases in magnitude and appears to shift to a new center wavelength at 910 nm. Simultaneously, absorbency at all wavelengths below approximately 815 nm increases and a new feature is seen to form at 760 nm. It is commonly assumed that the changes in peak magnitude at 930 nm and at 760 nm can be proportionately graded between the fully oxygenated and fully deoxygenated states. Moreover, when the NIR band features are used, it is common practice to ignore the visible and ultraviolet band features.

The spectral characteristics of cerebral lipids have not been published. Prior work shows that animal fat absorbs significantly at 928 nm and ~1030 nm.

Table 1 itemizes the major NIR band absorbing constituents of cerebral tissue and their center wavelength properties.

Center wavelength	Constituent
737	Water
760	Deoxyhemoglobin
830	Cytochrome oxidase
840	Water
910	Deoxyhemoglobin
928	Lipid
930	Oxyhemoglobin
972	Water
1025	Lipid

Table 1. Constituents of brain spectra published in the current literature.

Using data obtained from the literature, the individually identifiable constituents of the NIR band have been characterized in a manner that allows a knowledge base to be constructed. The knowledge

base consists of a series of equations that characterize each of the absorbing features by their center wavelength, λ_c, and full width at half maximum ("FWHM"). The shape of an absorbing feature is assumed to have gaussian properties and is described as,

$$[OD]_{\lambda min..\lambda max} = h_c \mathrm{EXP}(-0.5((\lambda-\lambda_c)/FWHM)^2) \qquad (3)$$

where: $[OD]_{\lambda min..\lambda max}$ is a range of optical density, or absorbence, and is dimensionless; λ is wavelength, in nanometers; *FWHM* is the full width at half-maximum, in nanometers; and h_c is peak height; and λ_c it the peak center wavelength, in nanometers. Note that here h_c is a composite parameter equal to $\varepsilon_{max} cL$ identified in equation 2, and is, therefore, without dimensions. Thus, a compound tissue spectrum becomes the summation of the simple constituent features superimposed on an apparent baseline absorption attributed to light loss due to photon scattering. Equation 3 is replicated n times, for the n absorbency peaks occurring in the NIR window and a constant, *k*, is added. Thus, for a compound or complex spectrum, shape is defined as

$$[OD]_{\lambda min..\lambda max} = \sum_{i=1}^{n} (OD_\lambda)_n + k \qquad (4)$$

which describes the general case knowledge base. Baseline OD is assumed to be wavelength independent. To account for features outside of the 700-1100 nm band that overlap into it and contribute absorption, it

was assumed that features at 555 nm and 577 nm "splay" into the NIR band as a result of the high absorptive properties. A first model system, termed herein as Model A for descriptive purposes, was then devised on the basis of the features shown in Table 2.

Center Wavelength (nm)	**FWHM (nm)**	**Constituent**
555	116	Deoxyhemoglobin
577	40	Oxyhemoglobin
760	16	Deoxyhemoglobin
820	85	Cytochrome oxidase
840	5	Water
875	40	Cytochrome oxidase
907	13	Deoxyhemoglobin
920	125	Oxyhemoglobin
928	8	Lipid
972	25	Water
1025	29	Lipid

Table 2. Features of the first model system used to extract tissue hemoglobin saturation from *in vivo* collected head spectra.

Animal Studies and Surgical Procedures

All experiments described herein were pre-approved by the Animal Care and Use Committee of the Johns Hopkins University Medical Center. In 21 dogs, anesthesia was induced using a combination of sodium pentobarbital and fentanyl anesthesias, administered intravenously. Anesthesia was maintained using only fentanyl. Cannula were placed in the femoral arteries and veins to enable measurements of arterial blood pressure and to collect arterial blood samples. A small sized cannula was placed in the superior saggital sinus to collect samples of cerebral venous blood. All blood gases were measured using a standard laboratory blood gas analyzer (ABL, Radiometer Corporation, Copenhagen, DK). Hemoglobin saturation and content were measured on an OSM3 (Radiometer corporation, Copenhagen, DK). Brain tissue spectra were collected through exposed skull after the temporalis muscle was removed, by placing two fiber optic bundles directly on the skull surface. The "optodes", that is, the fiber bundles delivering and collecting light at the skull's surface, were sealed using light opaque black modeling clay.

Several protocols for data collection were used, depending upon the type of information sought.

Hypoxic-hypoxia: All animals were challenged with multiple levels of reduced inspired oxygen concentration. The order of administering the hypoxic gas mixtures was usually from normoxic levels to severely hypoxic levels, usually in five to eight decremental steps. At each level, steady-state conditions were a requirement before collecting paired arterial and cerebral venous blood samples for analysis. A sample spectrum was collected either before or after the blood samples.

Hypercapnia: In twelve of these animals, CO2 was separately administered to induce tissue hyperoxygenation.

Anemic-hypoxia: In another two of the animals, anemic-hypoxia was induced by infusing two liters of lactated ringers while exchanging equivalent volumes of blood.

Hypothermia: In one animal, body temperature was cooled to 18 °C. Blood samples and spectra were collected during the period of body temperature reduction and after cooling was achieved graded hypoxia was induced stepwise to cover a large range of arterial blood hemoglobin saturations.

Figure 2 is a schematic illustration of the instrumentation 10 used with the above studies, and which could be used with the present

invention. Light is generated via a high intensity halogen lamp 13 powered by a power supply 14. The light 15 from lamp 13 is shined through a lens 16 into a Perkin Elmer FTIR 2000, Fourier transform spectrometer 18 (Model 2000, Perkin-Elmer Corp, Norwalk, CT) that was specially modified for this application by the instrument division of Perkin Elmer. The modifications allowed for the use of external light source 13 (Model 66183 halogen external light source; Oriel Instruments, Stratford, CT) and for the instrument to pass it's light output 15 to the input 20 of a 6-foot, 5 mm diameter, steel shielded fiber optic bundle 22, also known as an optode. The output end 24 of bundle 22 was placed in contact with the exposed skull 29 of an animal. Light 15 passing through the bundle was deposited on the skulls surface 32, whereby some photons migrated through the tissues of the skull, dura, cerebrospinal fluid, and brain 30, to exit at a distant site on the skulls' surface 28. A portion of the exiting light 26 was collected by a short, 3-foot length of shielded fiber optic bundle 34, also an optode, and passed to a peltier-cooled avalanche photodiode 36 ("APD"); (Advanced Photonix, Inc., Camarillo, CA). APD 36 is powered by a high voltage power supply 38. The signal from APD 36 was then passed to the control of a computer 40 after being filtered digitally by filter 42 (Model SR650, Dual channel, Highpass/lowpass Programmable Filter, Stanford Research Systems, Inc., Sunnyvale, CA). The data acquisition and timing schemes for light

generation and collection were software controlled. Additional software options allowed for control of the number of spectra collected, the number of scans averaged, and output aperture control using neutral density filtering. Post-hoc spectral processing was performed using Spectrum (Perkin-Elmer Corporation, Norwalk, CT) when necessary.

Data analysis and spectral decomposition

Decomposition analysis routines were written using two software packages. Manual curvefitting was performed using Sigmaplot for Windows, version 5.01 (Jandel Scientific, San Rafael, CA). Automated processing of bulk spectra was performed using a routine written for MatLab, version 4.0, (The Mathworks, Inc., Natick, MA). Using these software routines, Model A was applied to resolve h_c for each of the ten spectral features and baseline OD (k).

One of the goals of the study was to determine if a non-invasive measurement of tissue hemoglobin saturation could be computed from absorption spectra obtained from an animal's head. It must be kept in mind that the term "tissue hemoglobin saturation" is a construct that refers to the average saturation of hemoglobin of brain tissue expressed as a percentage of the total hemoglobin. In actuality there is no standard method for determining the value of this parameter. The term "tissue

hemoglobin saturation" stems from a literature citing that suggests approximately 75% of the blood volume of tissue is contained within the venous system. On this basis, it has been assumed by a number of laboratories that approximately 25% of the hemoglobin within a tissue is contained within the arterial compartment of the vasculature and that 75% is contained in the venous compartment. Thus, one may estimate a theoretical "standard" for comparative purposes. Realistically, the proportioning between compartments is probably not constant or uniform. For the study, a distribution of 10%:90% was arbitrarily selected, rather than the traditional 25%:75%. This was done because the final relationships between HbO2 / THb and the standard were nonlinear. Choosing a 10%:90% ratio appeared to linearize the relationship.

Herein the term "Standard $HbSat_{bt}$" refers to a computed value that is believed to represent the average percentage saturation of hemoglobin contained within a field that is defined by the migration path of photons shined into tissue. Standard $HbSat_{bt}$, computed as $0.1 * HbSat_{art} + 0.9 * HbSat_{cven}$, where $HbSat_{art}$ and $HbSat_{cven}$ are the percentage saturation of hemoglobin in arterial and cerebral venous blood, respectively. Standard $HbSat_{bt}$ was used to verify the NIR $HbSat_{bt}$ method. The features were resolved independently using a nonlinear curve-fitting algorithm constrained to yield only positive values for the peak height. Figure 3 is a

graph showing NIR prediction versus measured tissue hemoglobin saturation. Figure 3 shows that the ratio of optical attenuation at 920 nm to the sum of optical attenuations of 920 and 760 nm is linearly correlated to tissue hemoglobin saturation estimated as a weighted fraction of arterial and cerebral venous hemoglobin saturation. This figure also shows the results of fitting 180 absorption spectra, collected in 21 dogs, to constituent Model A. Thirty-seven spectra were collected in normoxic-normocapnic conditions (NN; Pa_{co2} =31-42 mmHg); 98 during conditions in which hypoxis-hypoxia was induced (HH; Pa_{o2} 8 – 100 mmHg); 26 during hypercapnia (HC; Pa_{co2} > 40 mmHg; 4 during anoxia (AX; $Pa_{o2<}$ 8mmHg; 8 in conditions where vascular hemoglobin concentration was varied (AH; (Hb)a 9-20 g/dl); and 7 during hypothermia (LT; rectal temperature <30°C). The correlation observed in each sorted condition was not different from the correlation established using pooled data. Figure 3 further shows that the ratio 50 $tHbO_2$/THb is proportional to $HbSat_{bt,}$ over the entire standard $HbSat_{bt}$ range 52. However, Figure 4 shows when the constituents were split out and plotted against the standard 48, it was found that both oxyhemoglobin 46 and deoxyhemoglobin 47 were inversely proportional to tissue hemoglobin saturation 48. Although this is theoretically possible in special conditions, (*e.g.*, when the fractional extraction of oxygen across the

brain decreases), the measured extraction fraction indicates such a change could not occur. It was concluded that the oxyhemoglobin measure, computed using Model A, yielded an erroneous result. It was reasoned that such an error could arise from cross-talk between oxyhemoglobin and another constituent. The most likely candidate for cross-talk is the secondary deoxyhemoglobin peak that overlaps the oxyhemoglobin spectrum. In Model A, h_c for the secondary peak was resolved as though the variable was independent of all other variables. In fact, it's value is related to that of the 760 nm variable, because the two peaks are part of the same complex spectrum.

The model system was revised to include two rules. First, it was assumed that the deoxyhemoglobin feature at 907 nm was not independent of the feature at 760 nm, but rather changed proportionately with the 760 nm feature. Secondly, the location of the feature was refined. In a small group of test data, the location was determined to be 937 nm, rather than the previously published 907 nm. Hence, a rule, $h_{937nm,} = \alpha\, h_{760nm,}$ was added to the model to account for the linkage, where α is a proportionality constant taken as the ratio of two specific absorption coefficients at the two wavelengths.

A second change was made in the model system to account for the shoulder region discussed previously when it was found that the 555 nm

and 577 nm features are better characterized as lorentzian shapes, than as gaussian shapes. As such, these features probably do not contribute significantly to the NIR band. However, the features of the ultraviolet band appear to be of such magnitude that they may still be recognizable in and contribute tilt to, NIR band spectra. Thus, it was decided to emulate the ultraviolet features using a singular gaussian-shape having a center location of 391 nm and a FWHM of 150 nm. Although 391 nm is well above the known location of the ultraviolet features, this value provided the best fit in a test dataset when the center wavelength of a single gaussian-shaped peak was assumed and it's FWHM resolved as an independent variable.

The revised model system, Model B, was reapplied to the previously-collected spectral library. The results are shown in Figures 5, 6, and 7. Figure 5 shows recovered optical attenuations due to different hemoglobin constituents – pooled results from fitting to Model B. To prevent cross-talk between overlapping oxy- and deoxyhemoglobin peaks in the 920-940 nm region, the deoxyhemoglobin peak at 937 nm was linked to the deoxyhemoglobin peak at 760 nm. In this fitting result, the linkage forces a solution where attenuation of 937 nm is 0.6 times attenuation at 760 nm. The effect on the recovered oxyhemoglobin attenuation 60 is such that a reduction in this parameter value is observed

as tissue hemoglobin saturation is reduced. In contrast, deoxyhemoglobin 62 rises.

Figure 6 shows the ratio 64 formed as attenuation due to oxyhemoglobin to the summed attenuations due to oxy- and deoxyhemoglobin is a linear function 66 of standard tissue hemoglobin 68. The effect of linking the primary and secondary deoxyhemoglobin peaks and forcing a common solution, is to steepen the slope of the correlation.

Figure 7 shows the Model B prediction of $HbSat_{bt}$. Tissue hemoglobin saturation 70 can be predicted from recovered optical densities at 920 and 760 nm (see Eq 5). A prediction equation of the form

$$NIRSat_{bt} = \frac{OD_{920nm} - c_1(OD_{920nm} + OD_{760nm})}{c_2\,(OD_{920nm} + OD_{760nm})} \qquad (5)$$

can be written. The coefficients c_1 and c_2 are the intercept and slope, respectively, of the tHbO2/THb ratio to the standard tissue hemoglobin saturation plot. The values of c_1 and $c_{2'}$ used to adjust the correlationship to the line of identity, were 0.4284 and 0.0046, respectively, for this dataset. In a population of 21 animals, the standard error of prediction if 6.5%. Prediction error is least at tissue saturations greater than 30%. Below this level the error of prediction is increased, but it is presently

unclear as to whether the fault lies with the model, or with the estimate used as the standard of comparison.

Referring again to Figure 5, Model B yielded relationships for deoxyhemoglobin and oxyhemoglobin that were directionally correct, *i.e.*, when tissue hemoglobin saturation 58 is high, tissue oxyhemoglobin 60 is high and tissue deoxyhemoglobin 62 is low, and when tissue hemoglobin saturation 58 is low, tissue oxyhemoglobin 60 is low and tissue deoxyhemoglobin 62 is high. The sum of the two hemoglobin parameters was inversely related to tissue hemoglobin saturation during hypoxic conditions and directly proportional to tissue hemoglobin saturation during hypercarbia (data not shown). This is consistent with hypoxia induced vasodilation and hypercarbia induced vasodilation; given that both are initiated from the normoxic-normocarbic state. As was observed using Model A, Model B yielded an overall excellent linear relationship between the ratio of the 920 nm constituent to the sum of the 920 nm and the 760 nm constituents (tHbO2/THb).

Figures 8A and B illustrate the best and worst fit cases. The left panel, Figure 8A, illustrates a correlation between Model B predicted tissue hemoglobin saturation 74 and the standard of comparison 72 for an animal with a large index of correlation. The right panel, Figure 8B,

illustrates the worst fit encountered. Overall, the standard error of prediction of 6.5 was realized.

In a subset of these experiments, optode separation distance was varied and the relative magnitude of absorbency in the deoxyhemoglobin, oxyhemoglobin, and water features expressed against standard tissue hemoglobin saturation (Figure 9). As expected from the modified Beer-Lambert relationship, and as shown in Figure 9 the optical attenuation 76 attributed to each recovered constituent 78 is a linear function of optode separation distance 80. This strongly supports the contention that h_c is a composite parameter, dependent in part upon pathlength (see Eq 2). As such, the absolute concentration of the recovered constituent can be calculated using a differential pathlength factor and appropriate molar extinction coefficient. In Figure 9, h_c for water (triangles), oxyhemoglobin (diamonds), and deoxyhemoglobin (squares) is plotted against the distance between the optodes at the time of measurement. Regression analysis shows that the y-axis intercept each correlationship is not different from the x,y axis intercept.

An advantage of using a ratioing method to compute tissue hemoglobin saturation is illustrated in Figure 10. Tissue hemoglobin saturation measurements are relatively insensitive to the distance between optodes. Because tissue hemoglobin saturation is computed as a ratio,

pathlength effects contained by in the numerator and denominator of the relationship tend to cancel. The method provides a measure that is optrode separation distance independent, *i.e.*, accurate measurement of optrode separation does not factor into the overall measurement error. In the population of dogs studied, tissue hemoglobin saturation measured using NIR technique during normoxic, normocarbic, normotensive conditions was 60.0% $\pm$SD 11.9% and did not significantly differ from standard tissue hemoglobin saturation (58.9% $\pm$ SD 9.1%).

An alternative and preferred model, Method C, for facilitating the spectral decomposition used to compute brain tissue hemoglobin saturation includes several revisions to the model used for Model B. First, the assignments of the 920 nm and 937 nm absorbencies are reversed. In Model B, the absorbency at 920 nm is attributed to oxyhemoglobin and the absorbency at 937 nm is attributed to a secondary deoxyhemoglobin peak. In addition, the FWHM for the two absorbencies is assigned values of 125 nm and 41 nm, respectively. However, after considering results obtained from fitting whole blood spectra, in the alternative and preferred model, these two absorbencies are reassigned to deoxyhemoglobin and oxyhemoglobin, respectively. In addition, a 41 nm FWHM is now applied when analyzing spectra obtained from either cat or dog. The FWHM used to resolve the 937 nm absorbency depends on

the animal species from which the spectra were collected. For cat spectra, a value of 175 nm yields the best fit to experimental data. For dogs, the fit is optimum when 130 nm is used to describe the peak. The physical basis for different FWHM requirements in the two species is unknown at this writing. These changes necessitate that the linkage between the 760 nm absorbency and the 937 nm absorbency also be revised, because the latter absorbency now represents oxyhemoglobin, rather than deoxyhemoglobin.

Second, the proportionality factor coupling the primary and secondary deoxyhemoglobin absorbencies is changed. Since the 760 and 920 nm absorbencies now both represent deoxyhemoglobin, they are coupled in the revised model using a proportionality factor valued at 1.09 for cats and 1.175 for dogs. The values were obtained by re-fitting the original data.

Third, the absorbency at 875 nm is now attributed to lipid. Originally, the absorbency requirement at 875 nm was considered to be a secondary peak in cytochrome c oxidase. Measurements taken from bacon 86 and from the white matter 88 of cat brain now identify a lipid contribution at this location. The absorption spectra shown in Figure 11 were collected by transilluminating a 1 cm sample chamber partially filled with either fat from bacon, or white matter collected from cat brain.

The spectra have been corrected for water content by differential spectroscopy. Absorption features are notable at 879, 928, and 1038 nm in both spectra. The FWHM are listed as determined by curve-fitting each spectrum. The 928nm feature 90 in white matter is small in comparison to the feature 92 observed for bacon. It should be noted that the 879 nm features of both fat and cerebral white matter have smaller FWHM than are needed to resolve tissue spectra. Thus, other constituents probably overlap in this region. Possible candidates for this region are: a secondary peak of cytochrome oxidase, or a peak of cytochrome B.

Fourth, with the current wavelength and FWHM assignments, it is found that the coefficients, c_1 and c_2, are not required. Tissue hemoglobin saturation is computed as a simple ratioing of the two absorbencies:

$$NIRHbSat_{bt} = 100 \times OD_{937nm} / (OD_{760nm} + OD_{937nm}). \qquad \text{(Eq 4)}$$

After revising the 920 and 937 nm peaks, the coupling factor between the two deoxyhemoglobin absorbencies located at 760 nm and at 920 nm also must also be re-determined. In the re-fitting process it was determined that the coupling factor interacts with the FWHM used to resolve the 937 nm oxyhemoglobin peak. This interaction is a result of the overlapping nature of these two absorbers. Increasing the value of the

coupling coefficient assigns a larger portion of the oxyhemoglobin component to the secondary deoxyhemoglobin component, thus causing the slope of the relationship between $oxyHb_{(937nm)}/THb$ and measured $HbSat_{bt}$ to become greater. This can be offset in part by increasing the breadth of the oxyhemoglobin peak. This interplay allows a solution for tissue hemoglobin saturation that is not dependent upon correcting coefficients, such as c_1 and c_2. Figure 12 shows the result of fitting the fraction $OD_{937nm} / (OD_{760nm} + OD_{937nm})$ 94 to standard $HbSat_{bt}$ yields a fit that lies on the line of identity and has zero bias. Also, it is seen that Model C correlates the ratio of oxyhemoglobin 94 to total hemoglobin 96 over a range of zero to 1, thus eliminating the need for the adjusting coefficients c_1 and c_2. This relationship has a zero bias, but tends to yield a somewhat larger prediction error. Unlike Model B, error appears to correlate inversely with hemoglobin saturation level and at very low saturation, a solution for oxyhemoglobin cannot be resolved.

The consequences of changing the coupling factor on the other variables of the model are not obvious. The constituent most affected by the change is total hemoglobin. In Model B, the best-fit solution to the hemoglobin components 98 showed an increased absorbency in the combined hemoglobin forms 102 during hypoxic-hypoxia and during hypercapnia (Figure 13A). This observation is consistent with the

consensus of other reports. The revised model does not yield a similar result (Figure 13B). It suggests that attenuation attributable to hemoglobin 102 either remains unchanged, or decreases. (Figure 13B). The fitting of spectra 98 and 100 for models B and C, respectively, obtained during hypercarbia remain consistent between the two models. In both cases hemoglobin attenuation 102, and by inference, cerebral blood volume, increases. The different results reported by the two models may be based upon Model B's inability to fully quantify oxyhemoglobin. Because oxyhemoglobin was only partially resolved, the rise in deoxyhemoglobin during hypoxia in combination with the disproportionate representation of the oxyhemoglobin fall, yielded an apparent rise in total hemoglobin. The physiological literature, currently, does not offer an explanation for these differences. In support of the findings from the revised Model C, there is now a suggestion that the increase in blood flow during hypoxia is mediated through changing blood flow velocity, rather than volume changes. The data are consistent with this hypothesis.

Referring again to Figures 13A and B, the linkage needed to stabilize cross-talk between oxy-and deoxyhemoglobin biases the total hemoglobin parameter as an index of blood volume. Hypercapnia increases tissue hemoglobin saturation, because, by increasing cerebral

blood flow, oxygen delivery is increased with respect to oxygen consumption. In hypoxia, the resulting decrease in oxygen delivery to tissue stimulates a compensatory increase in cerebral blood flow that serves to buffer the change. In both instances, the rise in cerebral blood flow would be expected to be accompanied by corresponding increases in cerebral blood volume, and total hemoglobin content of the tissue. In both Figures 13A and 13B above, hypercapnia was the predominant cause for tissue hemoglobin saturations lying above 58%, and hypoxia was the predominant cause for tissue hemoglobin saturations lying below 58%. Thus, one expects a concave relationship with a minima at the normocapnic-normoxic value, 58%. This was observed when Model B parameters were used to recover constituent attenuations. However, by removing the artifact of cross-talk between oxyhemoglobin and deoxyhemoglobin via the 760 to 920 nm linkage, it is now seen that a tilting is introduced into the relationship such that hypoxia is not accompanied by blood volume increases.

The method of the present invention has application to other types of tissue besides brain tissue. Figures 14 and 15 illustrate the general nature of the model. Figure 14 shows an absorption spectrum 104 collected from the head of a cat and a Model C fit 106 to such spectrum. The overlay of the Model C fitted absorption spectrum 106, was

reconstructed from the absorption coefficients that were recovered during the fitting process. Brain spectra contain two notable features: a peak centered around 760 nm that is attributable to deoxyhemoglobin, and a peak centered around 972 nm that is attributable to water. Decomposition analysis, recovers information on eight additional constituent features, and in the process yields an excellent fit to the overall absorption spectrum. While the model was developed to decompose brain spectra, it works equally well when applied to absorption spectra collected from other tissues.

Figure 15 shows an absorption spectrum 108 collected from human gastrocnemius muscle and a Model C fit 110 to such spectrum. Despite the shape differences between these two spectra (brain and skeletal muscle), Model C was able to decompose spectra from skeletal muscle because the constituents of the two tissues are similar. The spectral features used to compute tissue hemoglobin saturation again include oxyhemoglobin, deoxyhemoglobin, water, lipid, cytochrome oxidase and a component for characterizing light loss due to scattering. Thus, it is expected that decomposition analysis will provide much additional information about hemoglobin saturation, hemoglobin content, lipid content, cytochrome oxidase redox state, and water content in a variety of organ specific tissues. In addition to the features seen in brain tissue

absorption spectra, absorption spectra contains a prominent triglyceride peak centered around 928 nm. Because the attributes of lipids and fats are included, Model C is also able to recover constituent information from this tissue. Hence, the method appears to be generally applicable across a variety of tissues and, it is expected, will find application in studies yet to be conceived.

Although the present invention has been described in terms of a particular embodiment, it is not intended that the invention be limited to that embodiment. Modifications of the disclosed embodiment within the spirit of the invention will be apparent to those skilled in the art. The scope of the present invention is defined by the claims that follow.

WHAT IS CLAIMED IS:

1. A method of measuring tissue oxygenation comprising:

collecting for said tissue a compound reflectance spectra,

decomposing said compound reflectance spectra into individual spectral features that can be used to compute tissue hemoglobin saturation,

using values for said spectral features attributable to oxyhemoglobin and deoxyhemoglobin to construct a ratio for quantifying the percentage of total hemoglobin that contains oxygen.

2. The method of measuring tissue oxygenation recited in claim 1 wherein said spectral features used to compute tissue hemoglobin saturation include said oxyhemoglobin and deoxyhemoglobin and water, lipid, cytochrome oxidase and a component for characterizing light loss due to scattering.

3. The method of measuring tissue oxygenation recited in claim 1 wherein the step of decomposing said compound reflectance

spectra into individual spectral features further includes using for said decomposition a rule set.

4. The method of measuring tissue oxygenation recited in claim 1 wherein the step of decomposing said compound reflectance spectra into individual spectral features further includes using for said decomposition a component for characterizing light loss due to scattering.

5. The method of measuring tissue oxygenation recited in claim 3 wherein the step of using the rule set includes using a first rule indicating that a first portion of the deoxyhemoglobin contribution to the feature overlapping the oxyhemoglobin contribution to the feature is a constant fraction of a second, non-overlapping of the deoxyhemoglobin contribution to the feature.

6. The method of measuring tissue oxygenation recited in claim 5 wherein the step of using the rule set further includes using a second rule indicating that the deoxyhemoglobin feature at a first wavelength changed proportionately with the deoxyhemoglobin feature at a second wavelength.

7. The method of measuring tissue oxygenation recited in claim 6 wherein the step of using the rule set further includes using a third rule

indicating that a deoxyhemoglobin feature at a third wavelength and a oxyhemoglobin feature at a fourth wavelength do not contribute significantly to said compound reflectance spectra using light energy in an NIR band.

8. The method of measuring tissue oxygenation recited in claim 1 wherein the step of collecting for said tissue a compound reflectance spectra is done using light energy in an NIR band.

9. The method of measuring tissue oxygenation recited in claim 1 wherein the step of constructing a ratio for quantifying the percentage of total hemoglobin that contains oxygen further includes deriving a prediction equation for tissue hemoglobin saturation, said prediction equation being:

$$NIRHbSat_{bt} = \frac{OD_{920nm} - c_1(OD_{920nm} + OD_{760nm})}{c_2\,(OD_{920nm} + OD_{760nm})}.$$

10. The method of measuring tissue oxygenation recited in claim 1 wherein the step of constructing a ratio for quantifying the percentage of total hemoglobin that contains oxygen further includes deriving a prediction equation for tissue hemoglobin saturation, said prediction equation being:

$NIRHbSat_{bt} = 100 \times OD_{937nm} / (OD_{760nm} + OD_{937nm})$.

11. The method of measuring tissue oxygenation recited in claim 1 wherein the step of collecting for said tissue a compound reflectance spectra is performed using a first optode for transmitting light to said tissue and a second optode for collecting light exiting from said tissue.

12. The method of measuring tissue oxygenation recited in claim 1 wherein the step of decomposing said compound reflectance spectra into individual spectral features is performed using a computer.

13. A method of measuring brain tissue oxygenation comprising:

collecting for said brain tissue a compound reflectance spectra using light energy in an NIR band,

determining for said brain tissue a model system including spectra feature database determined by decomposing said compound reflectance spectra into individual spectral features that can be used to compute tissue hemoglobin saturation,

using values for said spectral features attributable to oxyhemoglobin and deoxyhemoglobin to construct a ratio for quantifying the percentage of total hemoglobin that contains oxygen.

14. The method of measuring tissue oxygenation recited in claim 13 wherein said model system further includes a rule set and a definition regarding how light scattering in said tissue contributes to baseline absorption of said light energy by said brain tissue.

15. The method of measuring tissue oxygenation recited in claim 13 wherein the spectral features used to compute tissue hemoglobin saturation include said oxyhemoglobin and deoxyhemoglobin and water, lipid, and cytochrome oxidase.

16. The method of measuring tissue oxygenation recited in claim 14 wherein said rule set includes a first rule indicating that the deoxyhemoglobin contribution to the feature overlapping oxyhemoglobin will be a constant fraction of the non-overlapping feature.

17. The method of measuring tissue oxygenation recited in claim 16 wherein said rule set further includes a second rule using a proportionality factor to account for the coupling of a primary deoxyhemoglobin feature at a first wavelength with and a secondary deoxyhemoglobin feature at a second wavelength.

18. The method of measuring tissue oxygenation recited in claim 17 wherein said second rule is defined as $h_{937nm} = \alpha h_{760nm}$, where 937 nm

is the wavelength of the secondary deoxyhemoglobin feature, 760 nm is a wavelength of the primary deoxyhemoglobin feature, and α is a proportionality constant.

19. The method of measuring tissue oxygenation recited in claim 17 wherein said rule set further includes a third rule indicating that a deoxyhemoglobin feature at a third wavelength and a oxyhemoglobin feature at a fourth wavelength do not contribute significantly to said compound reflectance spectra using light energy in said NIR band.

20. The method of measuring tissue oxygenation recited in claim 17 wherein said rule set further included a fourth rule wherein an absorbency at 875 nm is attributed to lipid.

21. The method of measuring tissue oxygenation recited in claim 13 wherein the step of constructing a ratio for quantifying the percentage of total hemoglobin that contains oxygen further includes deriving a prediction equation for tissue hemoglobin saturation, said prediction equation being:

$$NIRSat_{bt} = \frac{OD_{920nm} - c_1(OD_{920nm} + OD_{760nm})}{c_2\,(OD_{920nm} + OD_{760nm})}.$$

22. The method of measuring tissue oxygenation recited in claim 13 wherein the step of constructing a ratio for quantifying the percentage of total hemoglobin that contains oxygen further includes deriving a prediction equation for tissue hemoglobin saturation, said prediction equation being:

$$NIRHbSat_{bt} = 100 \times OD_{937nm} / (OD_{760nm} + OD_{937nm}).$$

23. The method of measuring tissue oxygenation recited in claim 13 wherein a first absorbency at 920 nm is attributed to oxyhemoglobin and a second absorbency at 937 nm is attributed to a secondary deoxyhemoglobin peak.

24. The method of measuring tissue oxygenation recited in claim 23 wherein the first absorbency is assigned a 125 nm FWHM and the second absorbency is assigned a 41 nm FWHM.

25. The method of measuring tissue oxygenation recited in claim 13 wherein a first absorbency at 920 nm is attributed to a secondary deoxyhemoglobin and a second absorbency at 937 nm is attributed to oxyhemoglobin peak.

26. The method of measuring tissue oxygenation recited in claim 25 wherein the first absorbency is assigned a 41 nm FWHM and the second absorbency is assigned a 125 nm FWHM.

27. The method of measuring tissue oxygenation recited in claim 13 wherein the step of collecting for said tissue a compound reflectance spectra is performed using a first optode for transmitting said energy to said tissue and a second optode for collecting said energy exiting from said tissue.

28. The method of measuring tissue oxygenation recited in claim 13 wherein the steps of determining said model system and constructing said ratio are performed using a computer.

29. An apparatus for measuring tissue oxygenation comprising:

means for collecting for said tissue a compound reflectance spectra,

means for decomposing said compound reflectance spectra into individual spectral features that can be used to compute tissue hemoglobin saturation,

means for using values for said spectral features attributable to oxyhemoglobin and deoxyhemoglobin to construct a ratio for quantifying the percentage of total hemoglobin that contains oxygen.

30. The apparatus for measuring tissue oxygenation recited in claim 29 wherein said spectral features used to compute tissue hemoglobin saturation include said oxyhemoglobin and deoxyhemoglobin and water, lipid, cytochrome oxidase and a component for characterizing light loss due to scattering.

31. The apparatus for measuring tissue oxygenation recited in claim 29 wherein the means for decomposing said compound reflectance spectra into individual spectral features further includes a rule set that is used for said decomposition.

32. The apparatus for measuring tissue oxygenation recited in claim 29 wherein the step of decomposing said compound reflectance spectra into individual spectral features further includes using for said decomposition a component for characterizing light loss due to scattering.

33. The apparatus for measuring tissue oxygenation recited in claim 31 wherein said decomposition of said compound reflectance spectra into individual spectral features is for brain tissue and wherein

said rule set includes a first rule indicating that a first portion of the deoxyhemoglobin contribution to the feature overlapping the oxyhemoglobin contribution to the feature is a constant fraction of a second, non-overlapping of the deoxyhemoglobin contribution to the feature.

34. The apparatus for measuring tissue oxygenation recited in claim 33 wherein said rule set further includes a second rule indicating that the deoxyhemoglobin feature at a first wavelength changed proportionately with the deoxyhemoglobin feature at a second wavelength.

35. The apparatus for measuring tissue oxygenation recited in claim 34 wherein said rule set further includes a third rule indicating that a deoxyhemoglobin feature at a third wavelength and a oxyhemoglobin feature at a fourth wavelength do not contribute significantly to said compound reflectance spectra using light energy in an NIR band.

36. The apparatus for measuring tissue oxygenation recited in claim 29 wherein said collection for said tissue of a compound reflectance spectra is done using light energy in an NIR band.

37. The apparatus for measuring tissue oxygenation recited in claim 29 wherein said spectral features used to compute tissue hemoglobin saturation are for brain tissue and wherein said means for constructing said ratio for quantifying the percentage of total hemoglobin that contains oxygen further includes means for deriving a prediction equation for tissue hemoglobin saturation, said prediction equation being:

$$NIRHbSat_{bt} = \frac{OD_{920nm} - c_1(OD_{920nm} + OD_{760nm})}{c_2\,(OD_{920nm} + OD_{760nm})}.$$

38. The apparatus for measuring tissue oxygenation recited in claim 29 wherein said spectral features used to compute tissue hemoglobin saturation are for brain tissue and wherein means for constructing a ratio for quantifying the percentage of total hemoglobin that contains oxygen further includes means for deriving a prediction equation for tissue hemoglobin saturation, said prediction equation being:

$$NIRHbSat_{bt} = 100 \times OD_{937nm} / (OD_{760nm} + OD_{937nm}).$$

39. The apparatus for measuring tissue oxygenation recited in claim 29 wherein said means for collecting said tissue a compound

reflectance spectra includes a first optode for transmitting light to said tissue and a second optode for collecting light exiting from said tissue.

40. The apparatus for measuring tissue oxygenation recited in claim 29 wherein said means for decomposing said compound reflectance spectra into individual spectral features is a computer.

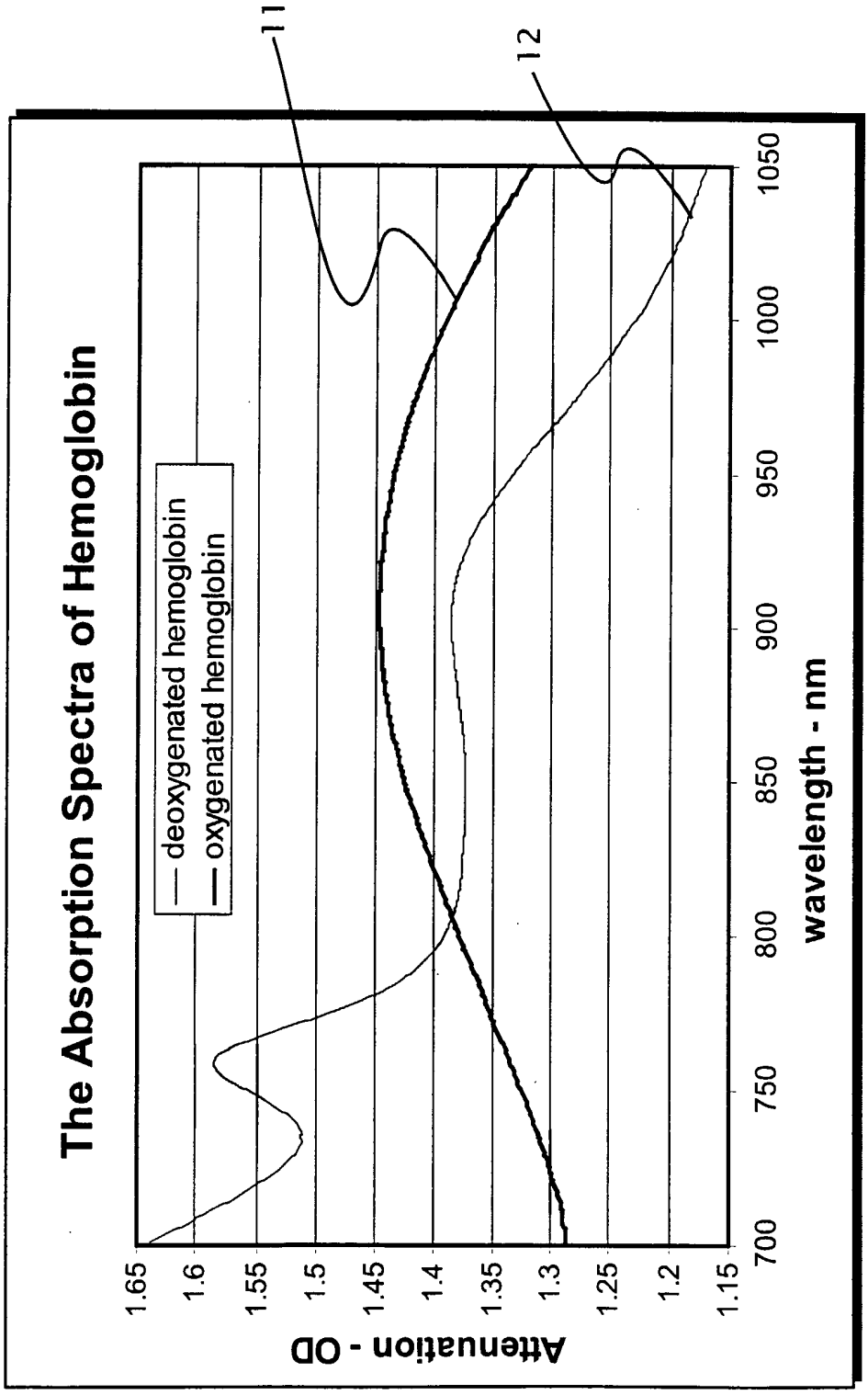
11
12
The Absorption Spectra of Hemoglobin
deoxygenated hemoglobin
oxygenated hemoglobin
Attenuation - OD
1.65
1.6
1.55
1.5
1.45
1.4
1.35
1.3
1.25
1.2
1.15
700
750
800
850
900
950
1000
1050
wavelength - nm

Fig. 1

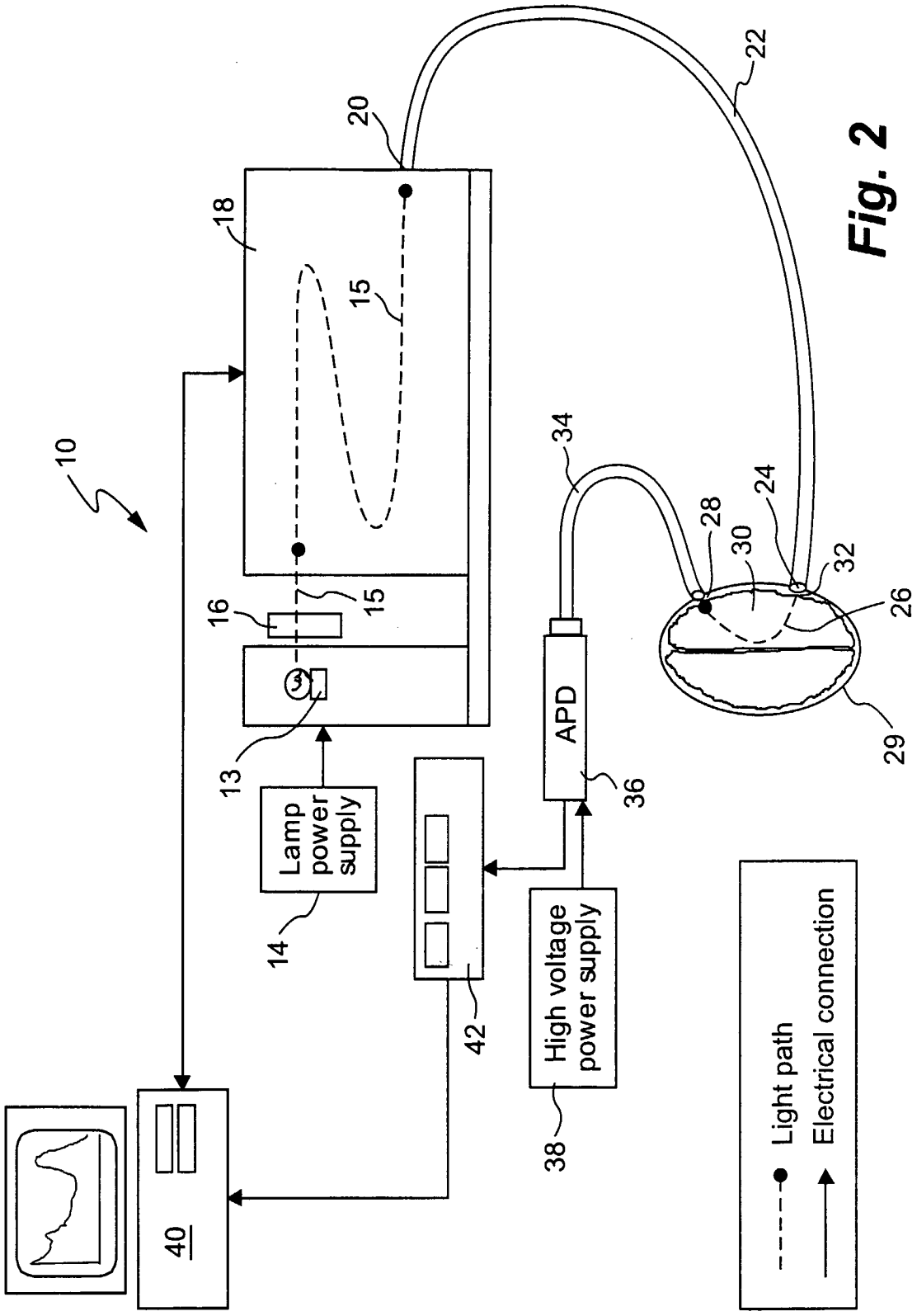
10
18
20
22
15
16
13
Lamp power supply
14
APD
34
36
24
28
30
32
26
29
42
High voltage power supply
38
40
Light path
Electrical connection

Fig. 2

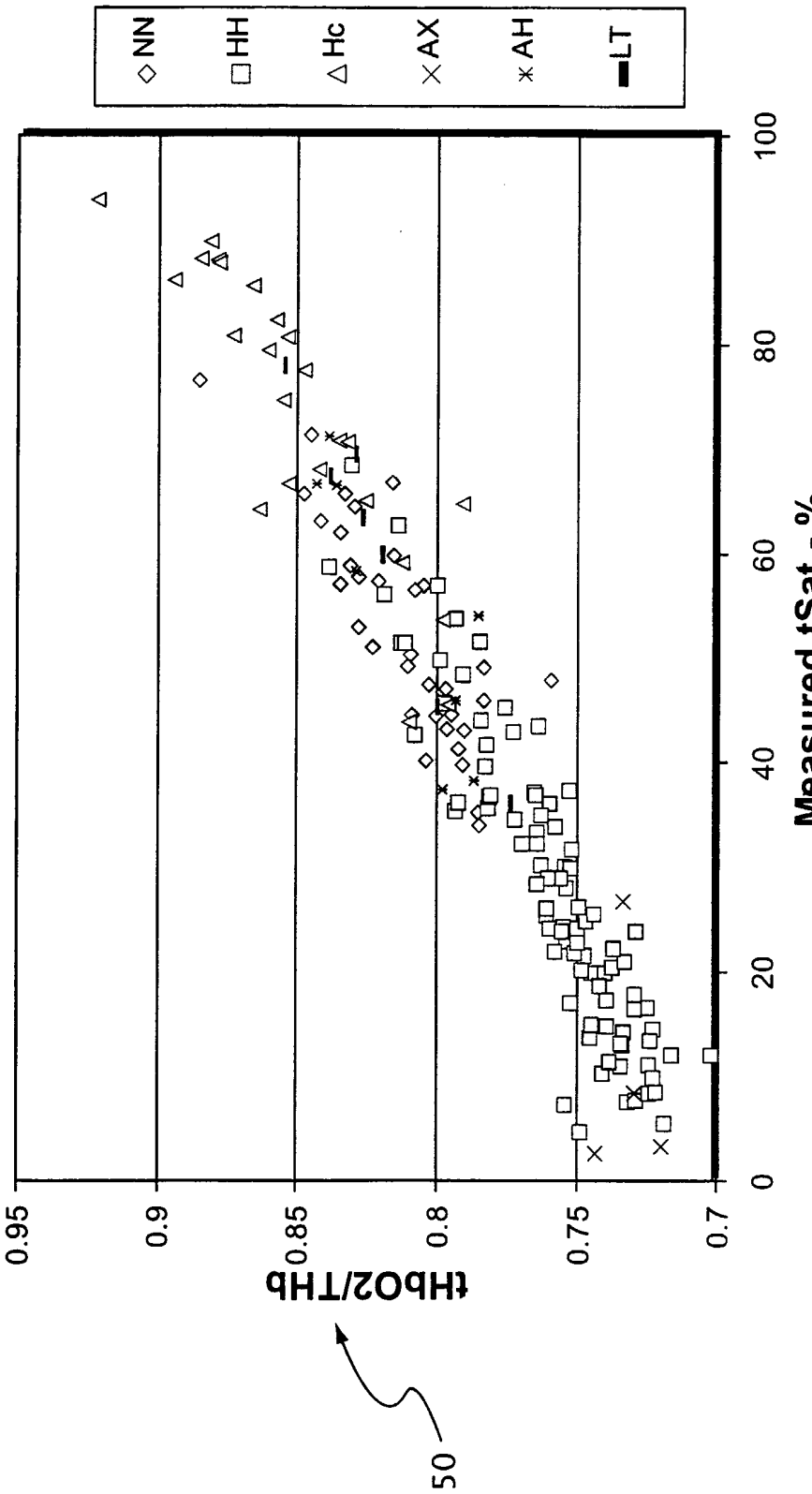
NN
HH
Hc
AX
AH
LT
tHbO2/THb
0.95
0.9
0.85
0.8
0.75
0.7
0
20
40
60
80
100
Measured tSat - %
50
52

Fig. 3

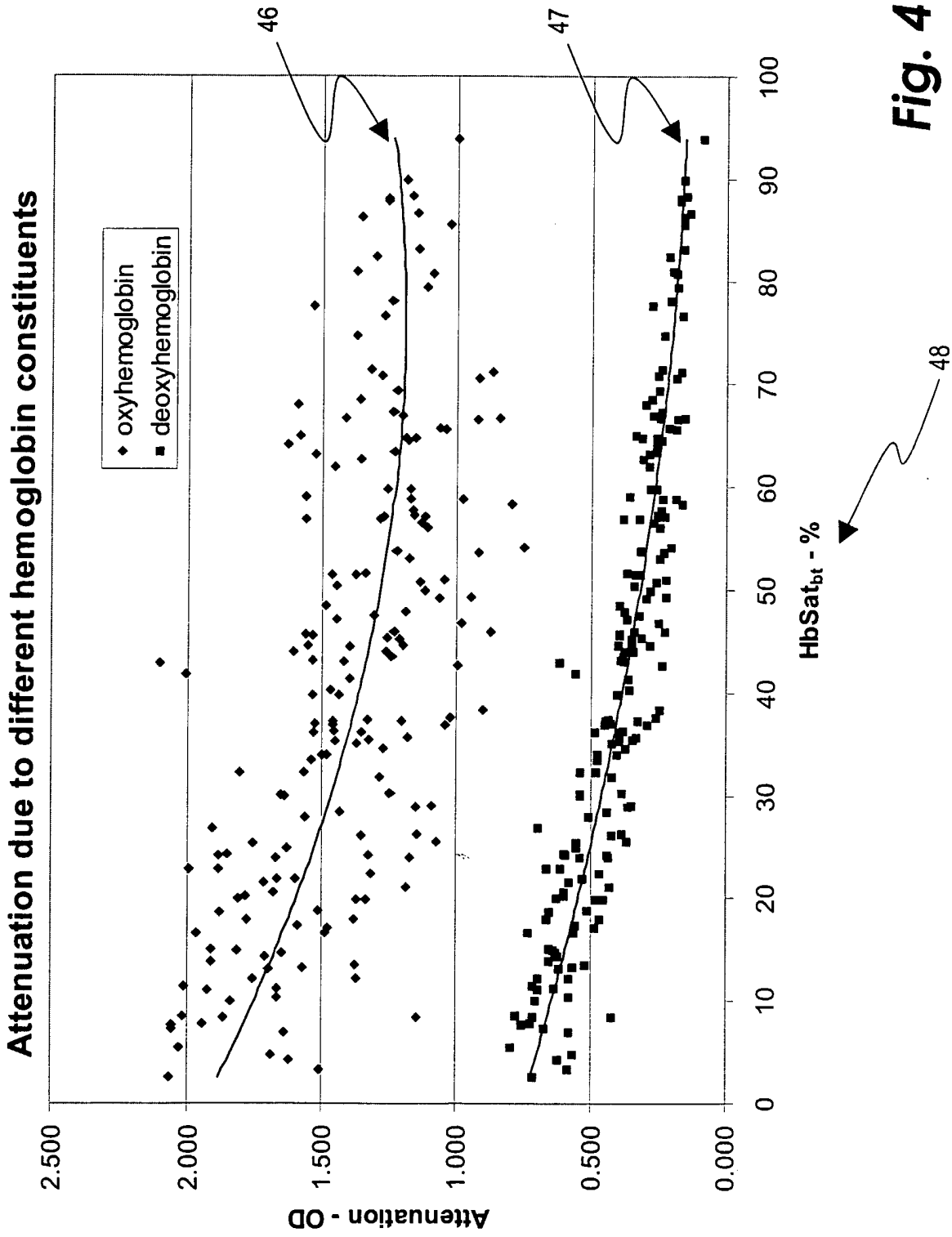
Attenuation due to different hemoglobin constituents
oxyhemoglobin
deoxyhemoglobin
46
47
48
Attenuation - OD
2.500
2.000
1.500
1.000
0.500
0.000
0
10
20
30
40
50
60
70
80
90
100
HbSat$_{bt}$ - %

Fig. 4

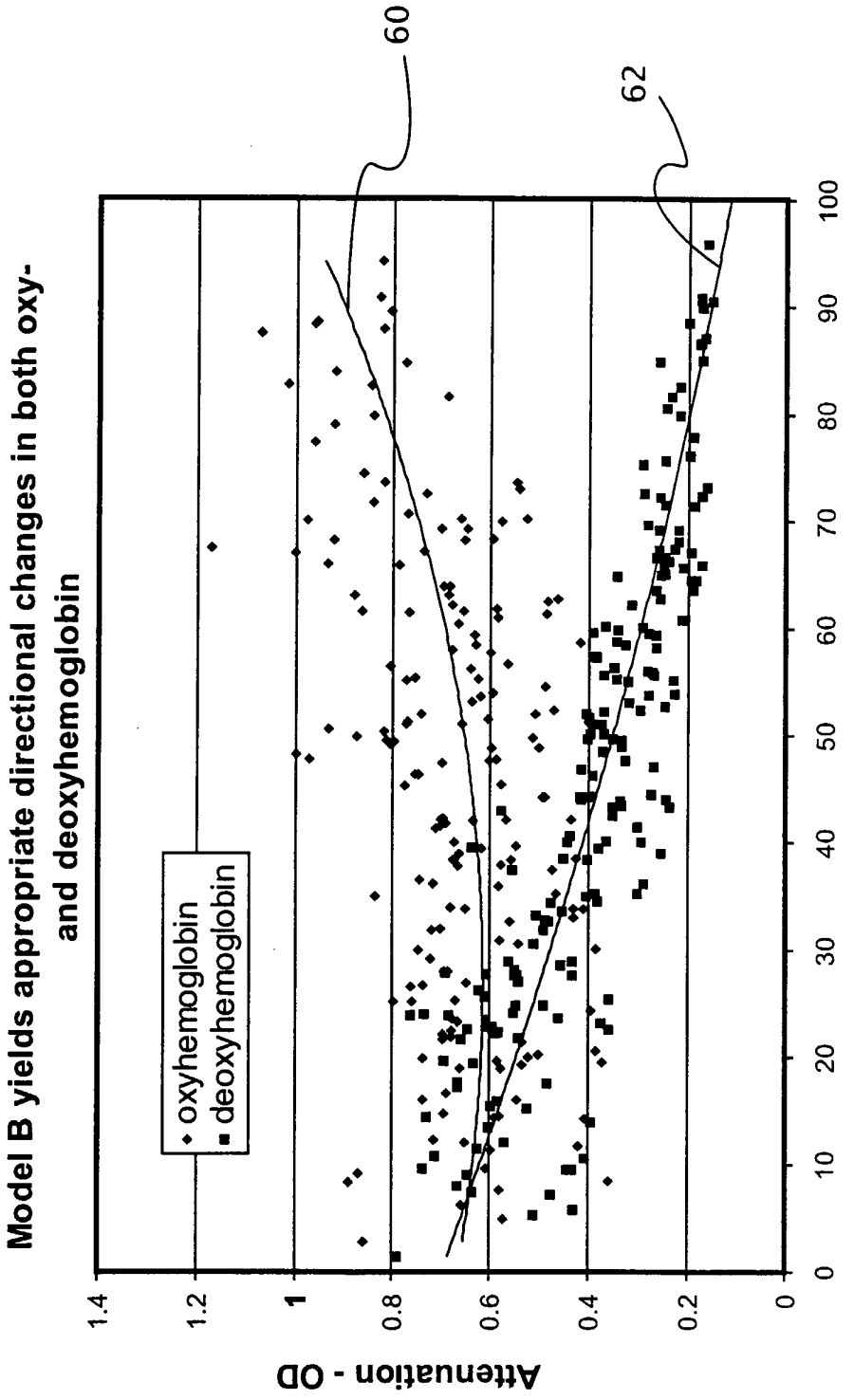
Model B yields appropriate directional changes in both oxy- and deoxyhemoglobin
oxyhemoglobin
deoxyhemoglobin
Attenuation - OD
1.4
1.2
1
0.8
0.6
0.4
0.2
0
HbSatbt - %
0
10
20
30
40
50
60
70
80
90
100
60
62
58

Fig. 5

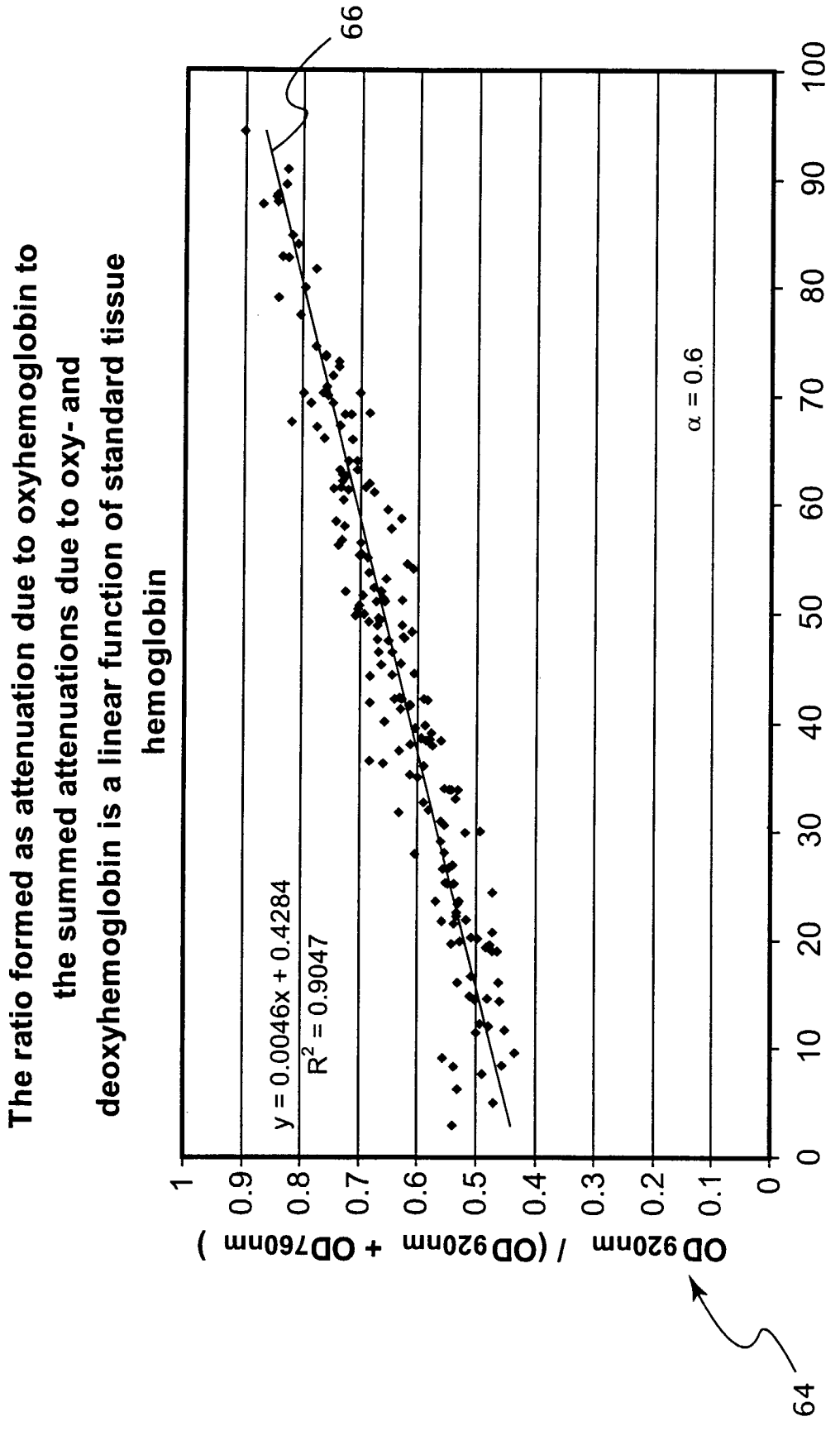
The ratio formed as attenuation due to oxyhemoglobin to the summed attenuations due to oxy- and deoxyhemoglobin is a linear function of standard tissue hemoglobin
66
64
68
OD920nm / (OD920nm + OD760nm)
HbSatbt - %
y = 0.0046x + 0.4284
R2 = 0.9047
α = 0.6
0
0.1
0.2
0.3
0.4
0.5
0.6
0.7
0.8
0.9
1
0
10
20
30
40
50
60
70
80
90
100

Fig. 6

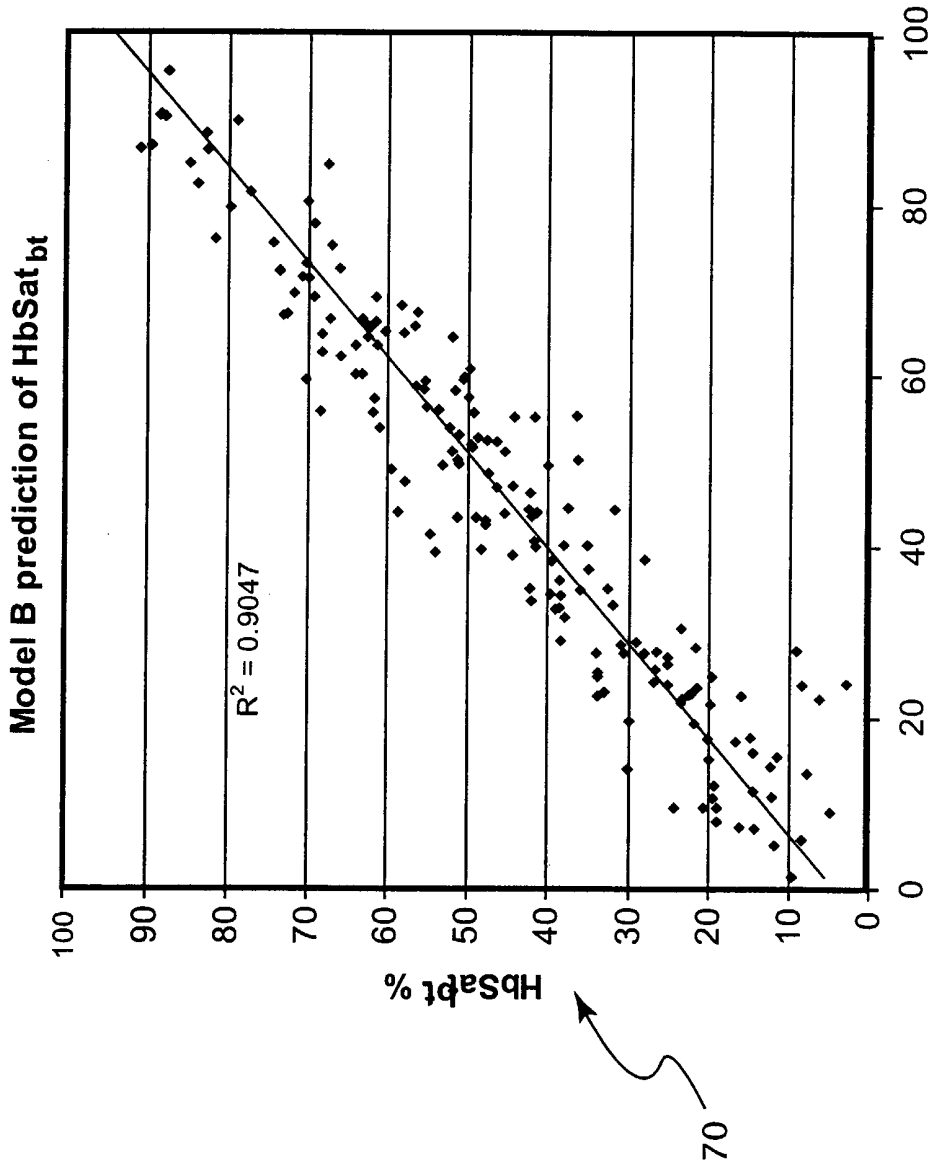
Model B prediction of HbSat$_{bt}$
R^2 = 0.9047
HbSat$_{bt}$ %
tSat$_{NIR}$ - %
0
10
20
30
40
50
60
70
80
90
100
0
20
40
60
80
100
70

Fig. 7

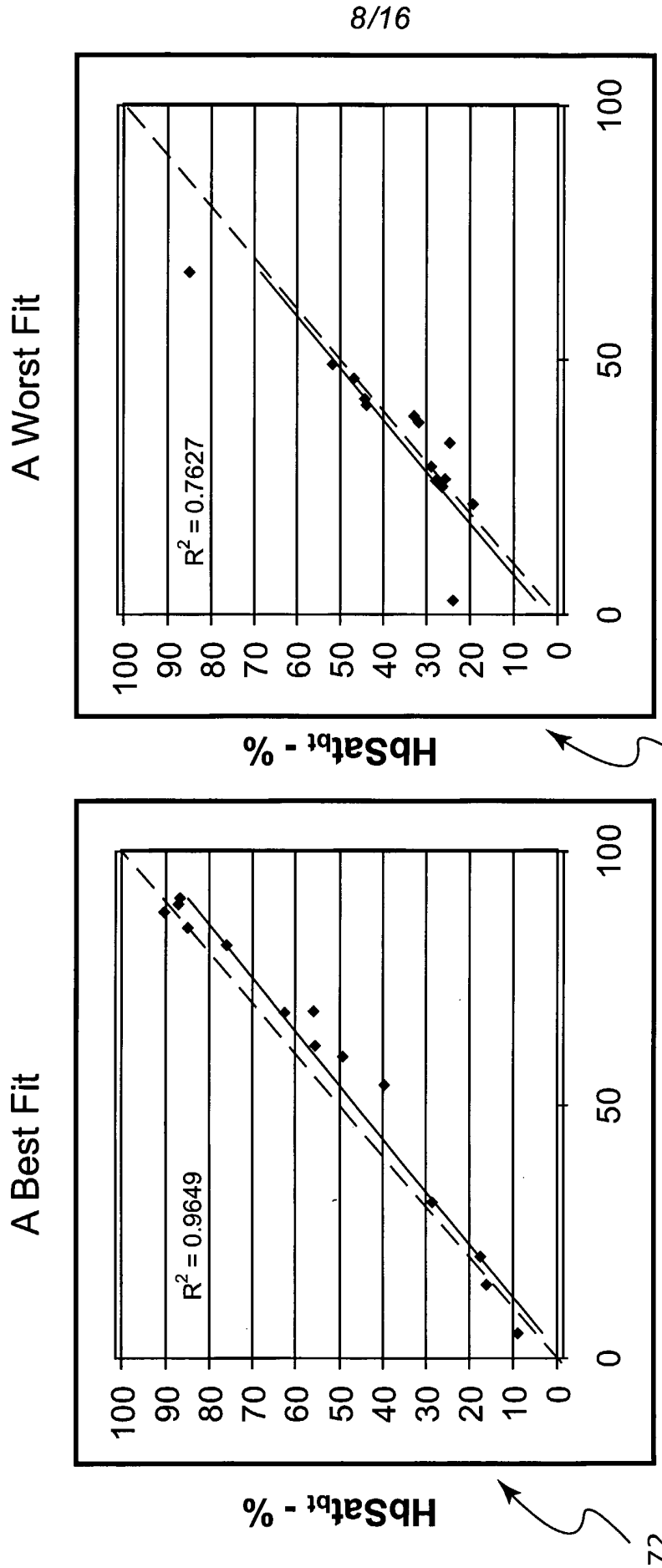
A Best Fit
$R^2 = 0.9649$
$HbSat_{bt}$ - %
$tSat_{NIR}$ - %
72
74
A Worst Fit
$R^2 = 0.7627$
$HbSat_{bt}$ - %
$tSat_{NIR}$ - %
72
74

Fig. 8A

Fig. 8B

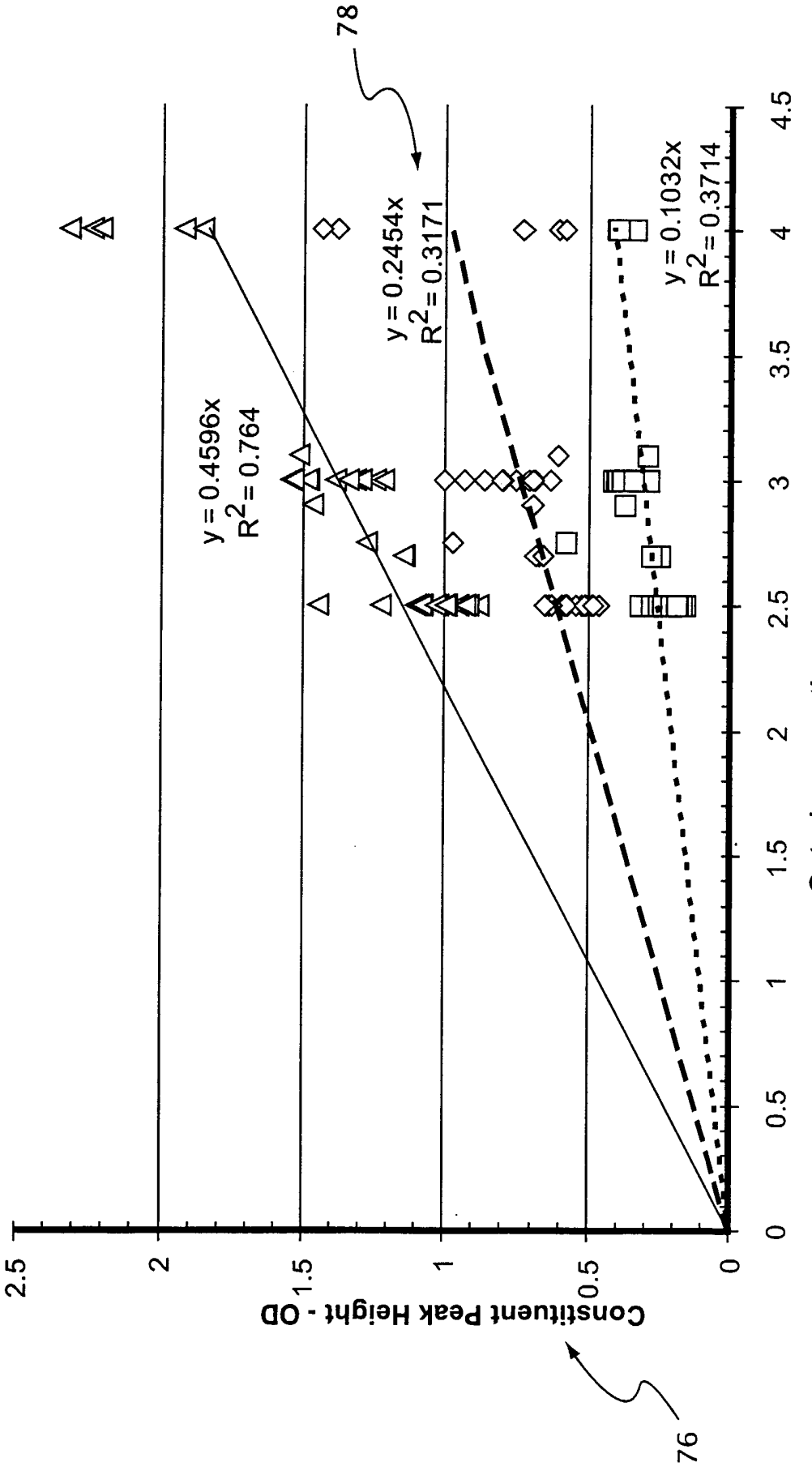
78
y = 0.4596x
R2 = 0.764
y = 0.2454x
R2 = 0.3171
y = 0.1032x
R2 = 0.3714
Constituent Peak Height - OD
Optode separation - cm
76
80
0
0.5
1
1.5
2
2.5
3
3.5
4
4.5

Fig. 9

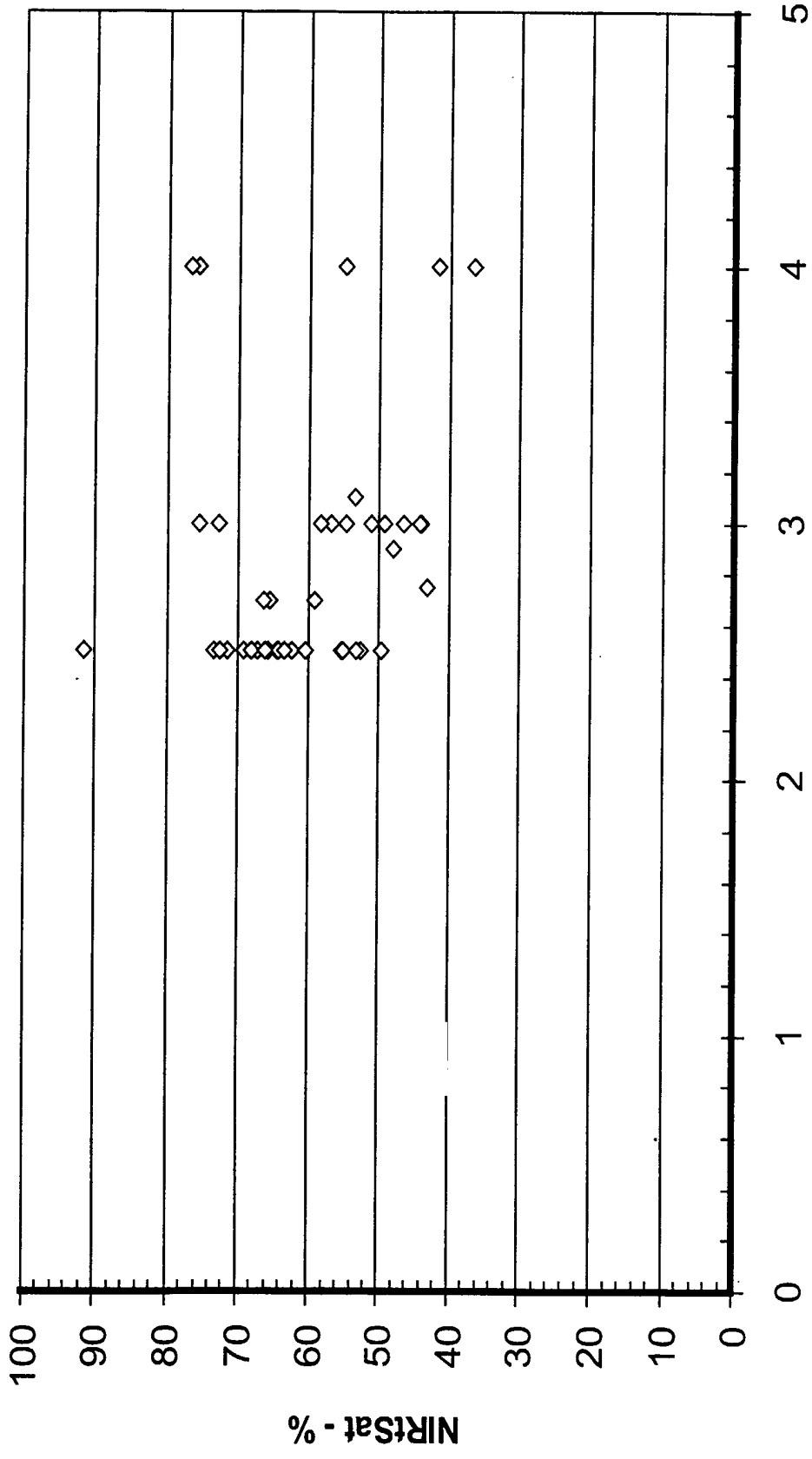
NIRtSat - %
100
90
80
70
60
50
40
30
20
10
0
0
1
2
3
4
5
Optode separation - cm

Fig. 10

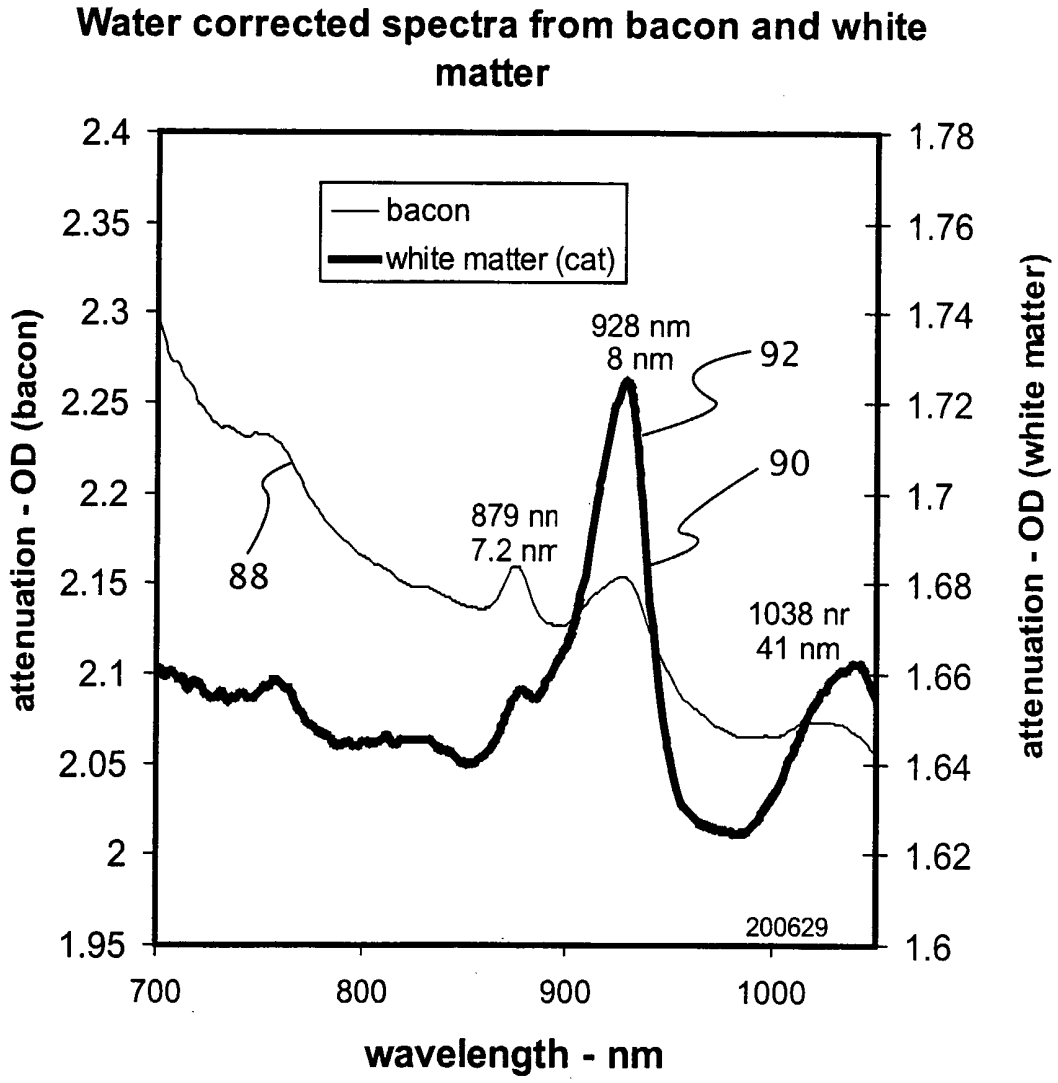
Water corrected spectra from bacon and white matter
bacon
white matter (cat)
928 nm
8 nm
92
90
879 nn
7.2 nm
88
1038 nr
41 nm
200629
attenuation - OD (bacon)
attenuation - OD (white matter)
wavelength - nm
2.4
2.35
2.3
2.25
2.2
2.15
2.1
2.05
2
1.95
1.78
1.76
1.74
1.72
1.7
1.68
1.66
1.64
1.62
1.6
700
800
900
1000

Fig. 11

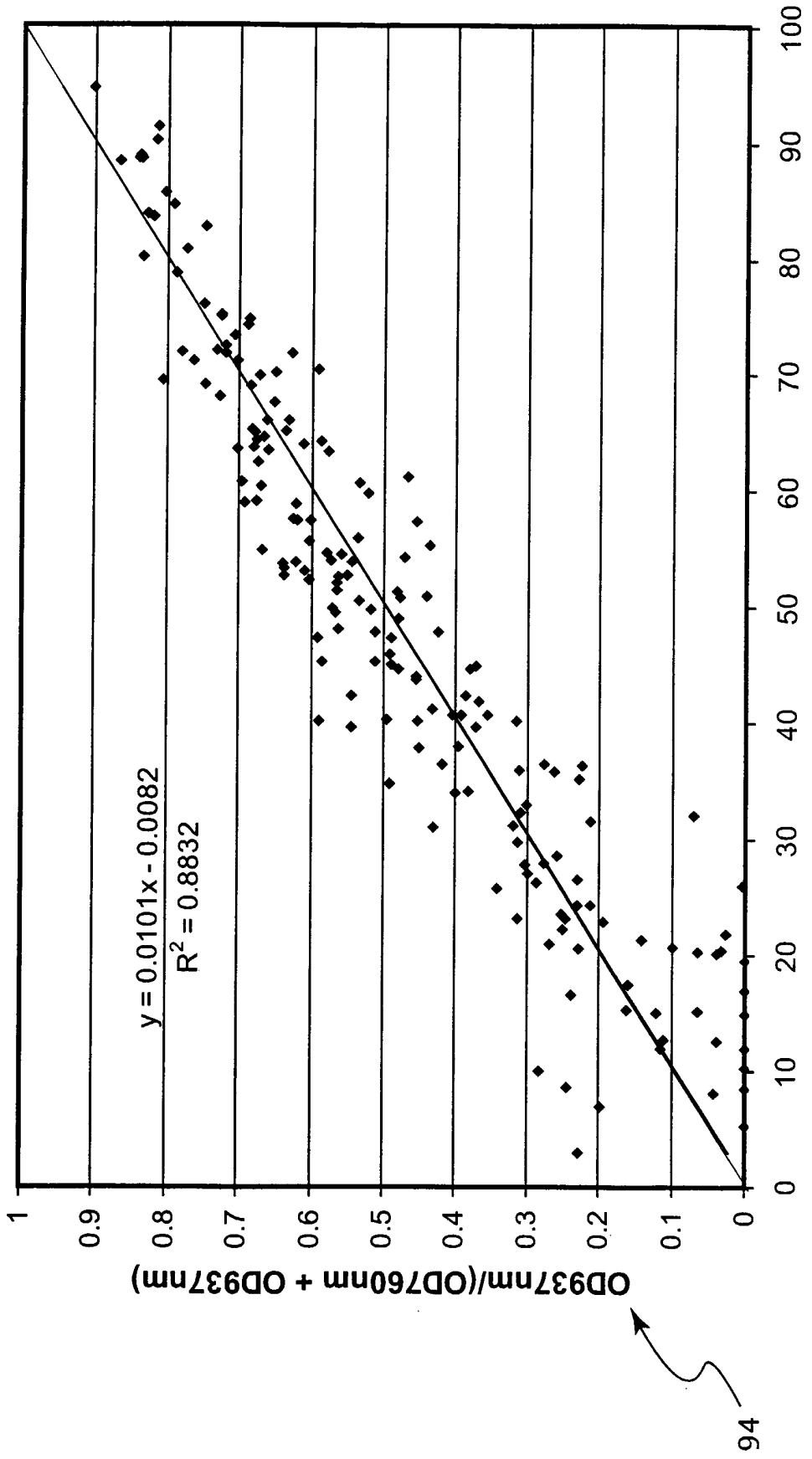
OD937nm/(OD760nm + OD937nm)
Computed tissue hemoglobin saturation - %
y = 0.0101x - 0.0082
R2 = 0.8832
94
96
0
0.1
0.2
0.3
0.4
0.5
0.6
0.7
0.8
0.9
1
0
10
20
30
40
50
60
70
80
90
100

Fig. 12

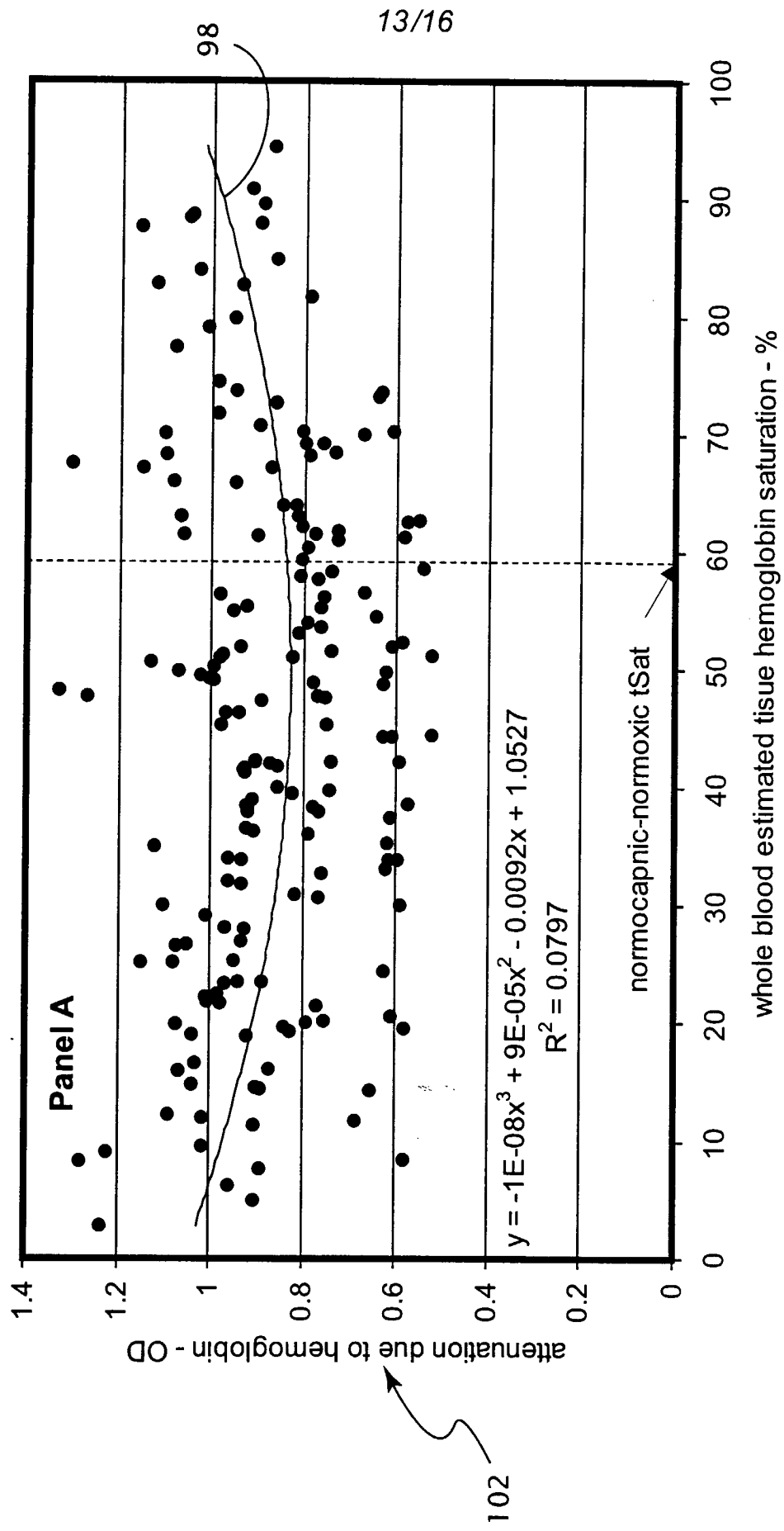
98
Panel A
y = -1E-08x^3 + 9E-05x^2 - 0.0092x + 1.0527
R^2 = 0.0797
normocapnic-normoxic tSat
attenuation due to hemoglobin - OD
whole blood estimated tisue hemoglobin saturation - %
0
0.2
0.4
0.6
0.8
1
1.2
1.4
0
10
20
30
40
50
60
70
80
90
100
102

Fig. 13A

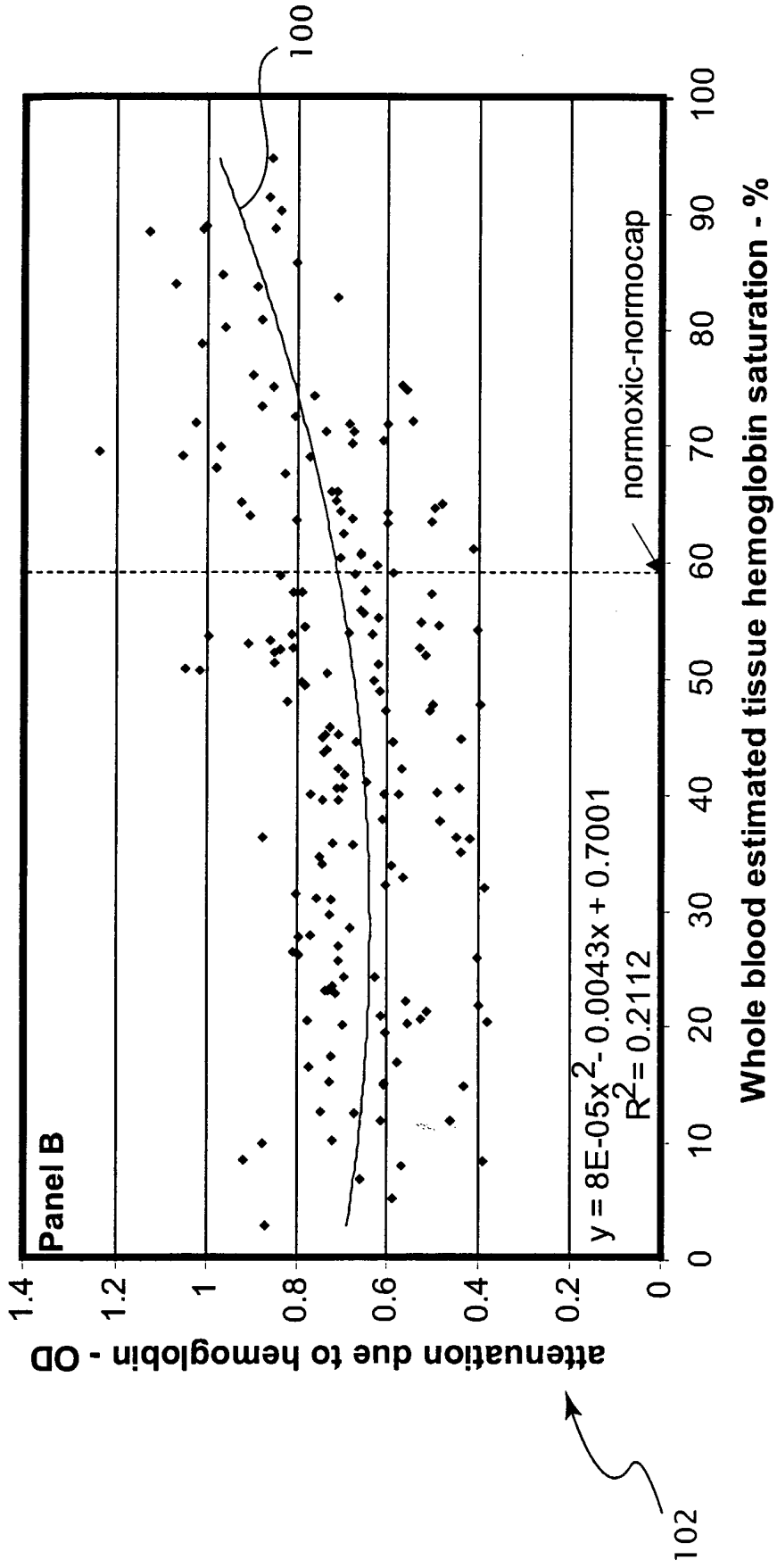
Panel B
attenuation due to hemoglobin - OD
Whole blood estimated tissue hemoglobin saturation - %
normoxic-normocap
y = 8E-05x2 - 0.0043x + 0.7001
R2 = 0.2112
100
102
0
0.2
0.4
0.6
0.8
1
1.2
1.4
10
20
30
40
50
60
70
80
90
100

Fig. 13B

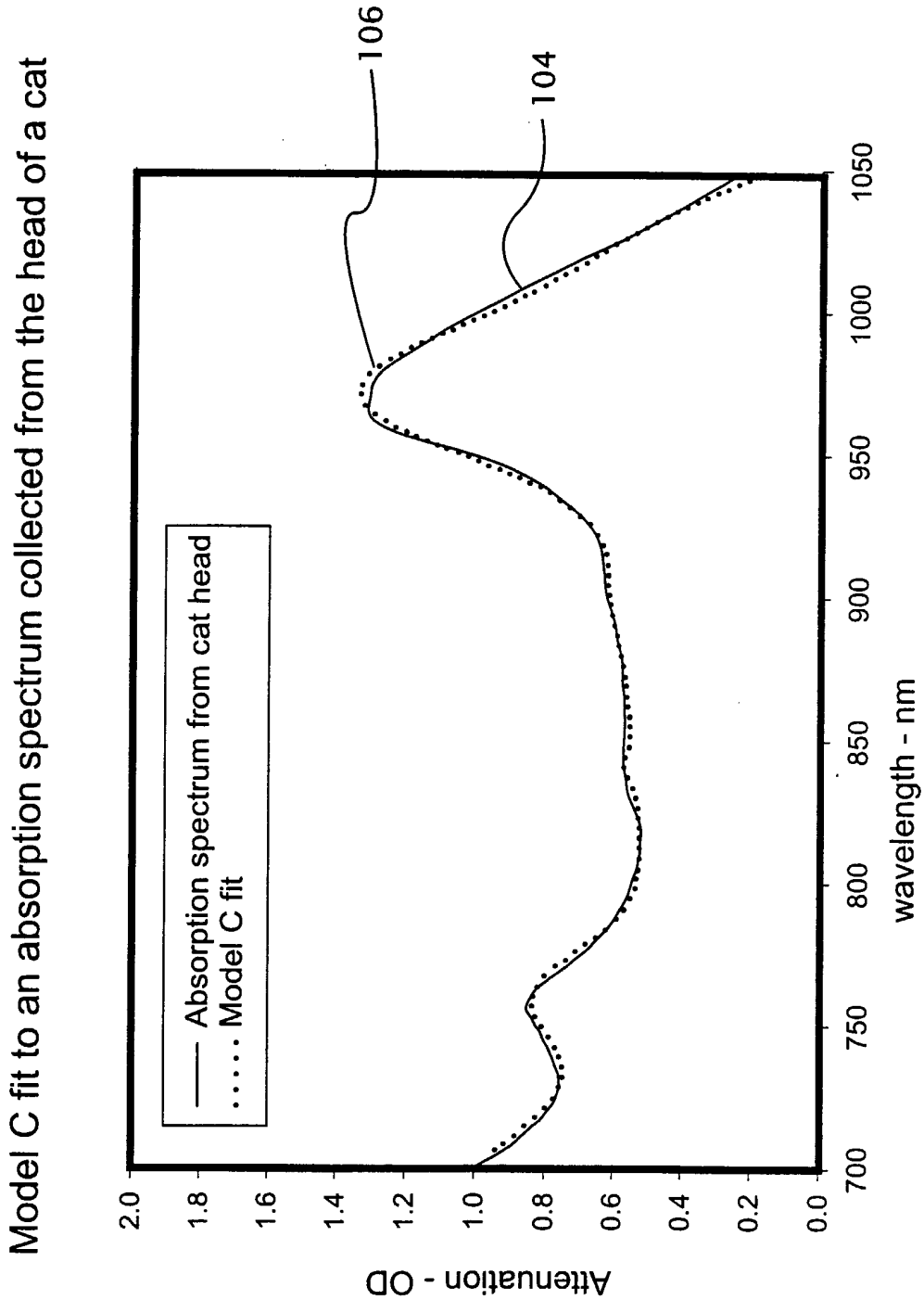
Model C fit to an absorption spectrum collected from the head of a cat
Absorption spectrum from cat head
Model C fit
106
104
Attenuation - OD
2.0
1.8
1.6
1.4
1.2
1.0
0.8
0.6
0.4
0.2
0.0
700
750
800
850
900
950
1000
1050
wavelength - nm

Fig. 14

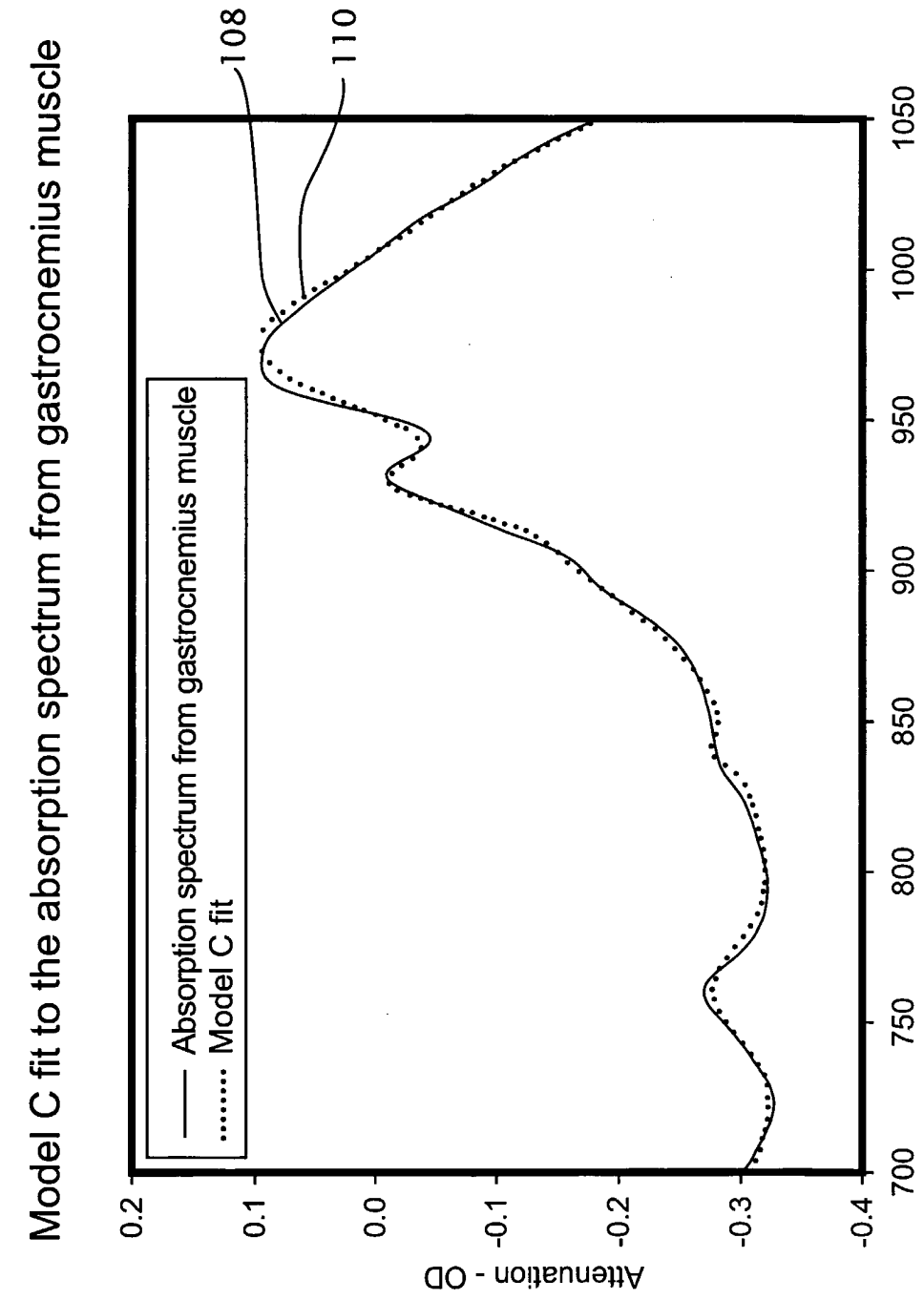
Model C fit to the absorption spectrum from gastrocnemius muscle
Absorption spectrum from gastrocnemius muscle
Model C fit
108
110
Attenuation - OD
0.2
0.1
0.0
-0.1
-0.2
-0.3
-0.4
700
750
800
850
900
950
1000
1050
wavelength - nm

Fig. 15

INTERNATIONAL SEARCH REPORT

International Application No
PCT/US 00/32830

A. CLASSIFICATION OF SUBJECT MATTER
IPC 7 G01N21/35 A61B5/00

According to International Patent Classification (IPC) or to both national classification and IPC

B. FIELDS SEARCHED

Minimum documentation searched (classification system followed by classification symbols)
IPC 7 G01N A61B

Documentation searched other than minimum documentation to the extent that such documents are included in the fields searched

Electronic data base consulted during the international search (name of data base and, where practical, search terms used)

EPO-Internal, WPI Data, COMPENDEX, INSPEC, PAJ

C. DOCUMENTS CONSIDERED TO BE RELEVANT

Category °	Citation of document, with indication, where appropriate, of the relevant passages	Relevant to claim No.
X	US 5 743 262 A (LEPPER JR JAMES M ET AL) 28 April 1998 (1998-04-28) column 1, line 10 - line 14 column 26, line 37 - line 52; figure 9 --- -/--	1-4,8, 11-15, 27, 29-32, 36,39,40

[X] Further documents are listed in the continuation of box C.

[X] Patent family members are listed in annex.

° Special categories of cited documents :

"A" document defining the general state of the art which is not considered to be of particular relevance

"E" earlier document but published on or after the international filing date

"L" document which may throw doubts on priority claim(s) or which is cited to establish the publication date of another citation or other special reason (as specified)

"O" document referring to an oral disclosure, use, exhibition or other means

"P" document published prior to the international filing date but later than the priority date claimed

"T" later document published after the international filing date or priority date and not in conflict with the application but cited to understand the principle or theory underlying the invention

"X" document of particular relevance; the claimed invention cannot be considered novel or cannot be considered to involve an inventive step when the document is taken alone

"Y" document of particular relevance; the claimed invention cannot be considered to involve an inventive step when the document is combined with one or more other such documents, such combination being obvious to a person skilled in the art.

"&" document member of the same patent family

Date of the actual completion of the international search	Date of mailing of the international search report
8 March 2001	15/03/2001

Name and mailing address of the ISA	Authorized officer
European Patent Office, P.B. 5818 Patentlaan 2 NL – 2280 HV Rijswijk Tel. (+31-70) 340-2040, Tx. 31 651 epo nl, Fax: (+31-70) 340-3016	Scheu, M

Form PCT/ISA/210 (second sheet) (July 1992)

C.(Continuation) DOCUMENTS CONSIDERED TO BE RELEVANT

Category °	Citation of document, with indication,where appropriate, of the relevant passages	Relevant to claim No.
X	CLEVE E ET AL: "ANWENDUNG CHEMOMETRISCHER AUSWERTEMETHODEN IN DER NIR-SPEKTROSKOPIEZUM NACHWEIS VON SCHLICHTEMITTELN AUF TEXTILEN FLACHENGEBILDEN" TEXTILVEREDLUNG,CH,THURGAUER TAGBLATT, WEINFELDEN, vol. 30, no. 7/08, 1 July 1995 (1995-07-01), pages 169-172, XP000516930 ISSN: 0040-5310 the whole document	1-4,8, 11-15, 27, 29-32, 36,39,40
A	MATCHER S J ET AL: "ABSOLUTE QUANTIFICATION OF DEOXYHAEMOGLOBIN CONCENTRATION IN TISSUENEAR INFRARED SPECTROSCOPY" PHYSICS IN MEDICINE AND BIOLOGY,GB,TAYLOR AND FRANCIS LTD. LONDON, vol. 39, no. 8, 1 August 1994 (1994-08-01), pages 1295-1312, XP000458639 ISSN: 0031-9155 page 1303	3,5-7, 14, 16-20, 31,33-35
A	SCHENKMAN K A ET AL: "NEAR-INFRARED SPECTROSCOPIC MEASUREMENT OF MYOGLOBIN OXYGEN SATURATION IN THE PRESENCE OF HEMOGLOBIN USING PARTIAL LEAST- SQUARES ANALYSIS" APPLIED SPECTROSCOPY,US,THE SOCIETY FOR APPLIED SPECTROSCOPY. BALTIMORE, vol. 53, no. 3, March 1999 (1999-03), pages 325-331, XP000805994 ISSN: 0003-7028 figure 3	11,27,39
A	BENNI P B ET AL: "A NOVEL NEAR-INFRARED SPECTROSCOPY (NIRS) SYSTEM FOR MEASURING REGIONAL OXYGEN SATURATION" PROCEEDINGS OF THE ANNUAL NORTHEAST BIOENGINEERING CONFERENCE,US,NEW YORK, IEEE, vol. CONF. 21, 22 May 1995 (1995-05-22), pages 105-107, XP000557749 ISBN: 0-7803-2693-8 page 105, right-hand column, last paragraph -page 106, left-hand column	1,13,29
A	US 5 782 237 A (MANNHEIMER PAUL D ET AL) 21 July 1998 (1998-07-21) column 1, line 38 - line 53 column 2, line 23 - line 40 column 8, line 49 - line 67; table FIGURE	9,10, 21-23, 37,38

INTERNATIONAL SEARCH REPORT

Information on patent family members

International Application No
PCT/US 00/32830

Patent document cited in search report	Publication date	Patent family member(s)	Publication date
US 5743262 A	28-04-1998	AU 715345 B	20-01-2000
		AU 6033296 A	30-12-1996
		CA 2221384 A	19-12-1996
		CN 1192273 A	02-09-1998
		EP 0830582 A	25-03-1998
		JP 11505451 T	21-05-1999
		US 6110522 A	29-08-2000
		WO 9641151 A	19-12-1996
US 5782237 A	21-07-1998	US 5421329 A	06-06-1995
		AT 195063 T	15-08-2000
		AU 705934 B	03-06-1999
		AU 2236095 A	23-10-1995
		BR 9507265 A	07-10-1997
		CA 2186225 A	12-10-1995
		CN 1148794 A	30-04-1997
		DE 69518235 D	07-09-2000
		DE 69518235 T	01-03-2001
		EP 0754007 A	22-01-1997
		EP 0992214 A	12-04-2000
		ES 2148509 T	16-10-2000
		FI 963921 A	28-11-1996
		JP 10500323 T	13-01-1998
		NO 964143 A	29-11-1996
		NZ 283905 A	24-11-1997
		PT 754007 T	30-11-2000
		WO 9526676 A	12-10-1995